Hydrometeorological Observations and Modeling of an Extreme Rainfall Event Using WRF and WRF-Hydro during the RELAMPAGO Field Campaign in Argentina

SUJAN PAL,[a] FRANCINA DOMINGUEZ,[a] MARÍA EUGENIA DILLON,[b] JAVIER ALVAREZ,[c] CARLOS MARCELO GARCIA,[c] STEPHEN W. NESBITT,[a] AND DAVID GOCHIS[d]

[a] *Department of Atmospheric Sciences, University of Illinois at Urbana–Champaign, Urbana, Illinois*
[b] *CONICET, Servicio Meteorológico Nacional, Buenos Aires, Argentina*
[c] *Institute for Advanced Studies for Engineering and Technology (IDIT CONICET-UNC) and Exact, Physical and Natural Sciences College, National University of Córdoba (FCEFyN-UNC), Córdoba, Argentina*
[d] *National Center for Atmospheric Research, Boulder, Colorado*

(Manuscript received 4 June 2020, in final form 5 October 2020)

ABSTRACT: Some of the most intense convective storms on Earth initiate near the Sierras de Córdoba mountain range in Argentina. The goal of the RELAMPAGO field campaign was to observe these intense convective storms and their associated impacts. The intense observation period (IOP) occurred during November–December 2018. The two goals of the hydrometeorological component of RELAMPAGO IOP were 1) to perform hydrological streamflow and meteorological observations in previously ungauged basins and 2) to build a hydrometeorological modeling system for hindcast and forecast applications. During the IOP, our team was able to construct the stage–discharge curves in three basins, as hydrological instrumentation and personnel were successfully deployed based on RELAMPAGO weather forecasts. We found that the flood response time in these river locations is typically between 5 and 6 h from the peak of the rain event. The satellite-observed rainfall product IMERG-Final showed a better representation of rain gauge–estimated precipitation, while IMERG-Early and IMERG-Late had significant positive bias. The modeling component focuses on the 48-h simulation of an extreme hydrometeorological event that occurred on 27 November 2018. Using the Weather Research and Forecasting (WRF) atmospheric model and its hydrologic component WRF-Hydro as an uncoupled hydrologic model, we developed a system for hindcast, deterministic forecast, and a 60-member ensemble forecast initialized with regional-scale atmospheric data assimilation. Critically, our results highlight that streamflow simulations using the ensemble forecasting with data assimilation provide realistic flash flood forecast in terms of timing and magnitude of the peak. Our findings from this work are being used by the water managers in the region.

KEYWORDS: Flood events; Convective storms; Hydrometeorology; Forecast verification/skill; Hydrologic models; Mesoscale models; Precipitation

1. Introduction

Some of the world's deepest and largest convective storms develop at the foothills of the Sierras de Córdoba (SDC), a 2000-m north–south mountain range, east of the Andes, located in central Argentina (Zipser et al. 2006). These intense and frequent convective storms organize into mesoscale convective systems (MCSs) and then travel toward the eastern part of Argentina (Salio et al. 2002, 2007; Rasmussen and Houze 2011; Rasmussen et al. 2014; Vidal 2014; Mulholland et al. 2018), affecting the Carcarañá River basin, a subbasin of the La Plata River basin. As such, the mountainous headwater region of this basin (Fig. 1) is ideally suited to perform hydrometeorological studies of convection and flash flooding. To measure these intense convective storms and associated impacts, the Remote Sensing of Electrification, Lightning and Mesoscale/Microscale Processes with Adaptive Ground Observations (RELAMPAGO, https://www.eol.ucar.edu/field_projects/relampago) field campaign took place in west central Argentina in the general vicinity of the SDC near the city of Córdoba and the Andes foothills near the city of Mendoza. The project consisted of an extended hydrometeorology observing period (EHOP) from 1 June 2018 to 30 April 2019 and an intensive observing period (IOP) from 1 November to 16 December 2018. Here we focus on results from the IOP. The overarching objectives of the RELAMPAGO project were to 1) characterize the preconvective and convective environments; 2) characterize thermodynamic and microphysical properties of clouds and precipitation, convective outflow, lightning, and hail events; and 3) observe hydrometeorological interactions with convective systems (Nesbitt 2016). The occurrence of convective events in this region is linked to the strengthening of topographically guided South American low-level jet (SALLJ), which brings moist air poleward, and strong convection is formed at the exit region controlled primarily by diabatic effects. Convective storms produce most of the austral summer precipitation in La Plata River basin (Rasmussen et al. 2016). This study performs a hydrometeorological analysis, flash flood observations, and modeling of an extreme MCS event that occurred during RELAMPAGO. This event, which took place on 27 November 2018, was one of the most extreme hydrometeorological events observed during the IOP. Based on

Supplemental information related to this paper is available at the Journals Online website: https://doi.org/10.1175/JHM-D-20-0133.s1.

Corresponding author: Francina Dominguez, francina@illinois.edu

DOI: 10.1175/JHM-D-20-0133.1

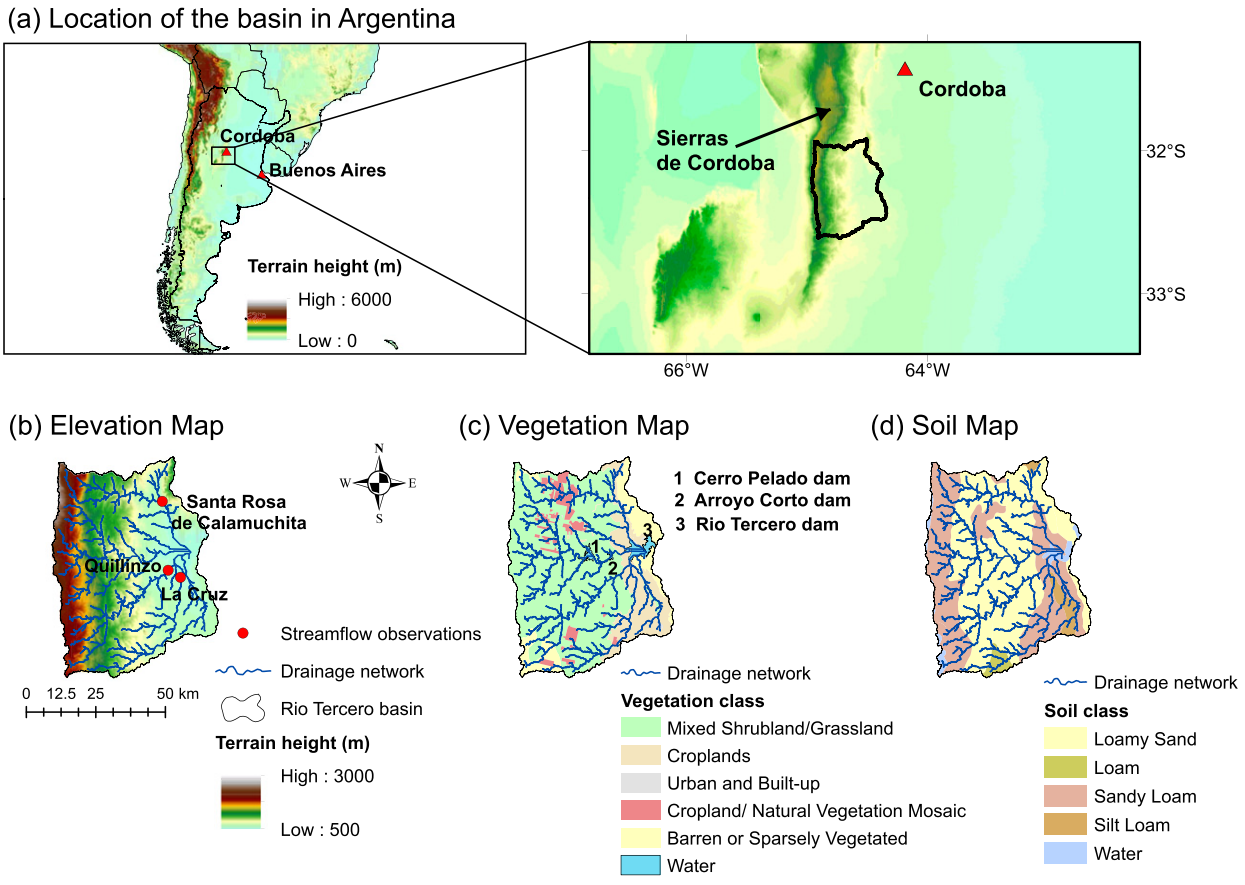

FIG. 1. (a) Location of Rio Tercero basin and Sierras de Córdoba mountain range in Argentina. (b) Elevation, drainage network, and locations of streamflow measurement (Santa Rosa de Calamuchita, Quillinzo, and La Cruz) in the basin. (c) Land cover classification and dam locations in the basin. (d) Soil texture classification at 20-arc-s resolution obtained from CIRSA-INA.

records of inflow water volume at Rio Tercero Dam (Fig. 1c), this event had a return period of 1 in 25 years.

Extreme rainfall events and associated flooding are some of the most pervasive weather-related natural hazards, having the potential to damage civil infrastructure, vegetation, and animal and human life globally (Noji and Lee 2005; Adikari and Yoshitani 2009). Flash floods, in particular, remain a severe threat to the society (French et al. 1983; Ashley and Ashley 2008; Rozalis et al. 2010; Tao et al. 2016). Flash floods are fast-flow-response events with short time-to-peak of a few hours (Georgakakos and Hudlow 1984; Tao and Barros 2013). This type of hydrometeorological phenomenon typically occurs in small streams of mountainous regions with sheer slopes and small catchment areas. High streamflow occurs shortly after extreme rainfall events associated with short deep convective storms with high rainfall intensity (Gruntfest and Huber 1991; Broxton et al. 2014). Factors affecting flash flood are 1) characteristics of rain (intensity, duration, amount, and time–space distribution) and 2) hydrological properties of the basin (area, length, slope, antecedent conditions, type of soil, and land use). Flash flood prediction at a subdaily scale remains a challenge in poorly gauged and remote basins, especially in mountainous regions (Reed et al. 2007; Norbiato et al. 2008; Band et al. 2012; Tao and Barros 2013).

The headwaters of the Carcarañá River are prone to flash flooding events. The most devastating recorded flood event occurred in March of 1919, as several towns were flooded causing economic losses in farmlands, and damages in civil infrastructure such as bridges, houses, and roads (https://www.eldiariodelcentrodelpais.com/2018/03/11/inundacion-de-1919/). Important flooding events also occurred in January 1981 and November 1993 (Colautti 2007). More recently, a chain of events in February 2014 affected the entire basin, ranking among the seven most devastating flood events in the province of Córdoba in the past 100 years (https://www.eldiariodelcentrodelpais.com/2018/03/11/inundacion-de-1919/). However, there is no quantitative hydrometeorological record of these events due to a lack of long-term observations.

This is the first study to analyze the flash flood response in the complex terrain of Córdoba, Argentina, resulting from some of the most intense storms on Earth. While severe convection in the region has been highlighted in past literature (Saulo et al. 2004; Saulo et al. 2007; Rasmussen and Houze 2016), flash floods resulting from these storms have not been previously analyzed, and the community is lacking a

forecasting framework to generate a reliable flood warning system. Prior to this project, there were no streamflow observations in the headwaters of the catchment, despite the societal and economic impacts of flash flooding in the region. The large-scale RELAMPAGO field campaign brought together hydrologists and atmospheric scientists to observe specific extreme convective events and their associated hydrologic impacts.

Within the scope of the RELAMPAGO IOP, the hydrometeorology group performed the first streamflow measurements in the headwaters of the basin using acoustic Doppler current profiler (ADCP) and large-scale particle image velocimetry (LSPIV). The group measured the hydrologic response of three severe high-flow events during the IOP. The main objectives of the hydrometeorological observations were 1) to quantify the hydrological response associated to the extreme convective events simultaneously measured by the larger RELAMPAGO team, 2) to build suitable stage–discharge curves for the headwater rivers that could be used by hydrologists and water resource managing community once the IOP ended, and 3) to use the observations to develop a process-based hydrological model to realistically capture the hydrologic response and eventually use it for forecasting.

Previous studies have shown that minimally calibrated, physics-based models perform well in different geographic regions across the globe and can be useful over ungauged areas (Michaud and Sorooshian 1994; Lange and Leibundgut 2000; Sivapalan et al. 2003; Smith et al. 2012). These types of flexible models can be robust in the sense that the output and forecasts from the model remains consistent, even when one or more of the input variables or assumptions are drastically changed due to unforeseen circumstances. Also, these could be employed in various watersheds, bypassing the need of extensive calibration over long periods. This is useful where a long-term streamflow record is unavailable. A physics-based and fully distributed hydrologic modeling approach is also useful in flood-prone watersheds, to evaluate the flood predictability and possible hydrologic response in a changing climate (Moore and Clarke 1981; Clark et al. 2008; Fenicia et al. 2011). For this study, we use the WRF-Hydro modeling system as an uncoupled (i.e., driven by independent meteorological forcing), distributed hydrologic model over the basin to assess its capability in a flash flood hindcast and forecasting framework. WRF-Hydro is currently the underlying framework for the National Water Model of the United States and has previously been used as a coupled and uncoupled hydrologic model for streamflow forecasting over different watersheds around the globe (Yucel et al. 2015; Senatore et al. 2015; Lin et al. 2018b; Fersch et al. 2020; Senatore et al. 2020). Recently, WRF-Hydro has been used for flash flood prediction in the United States [Gochis et al. (2015) in the Colorado Front Range, Lin et al. (2018a) in Texas, and Viterbo et al. (2020) in Maryland] and other regions worldwide [Ryu et al. (2017) in the Korean Peninsula and Varlas et al. (2019) in Greece]. Flash floods in the headwaters of the Carcarañá affect riverine communities and the larger region in terms of water resource management including operations of three major dams (Fig. 1c). Hence, a suitable hydrometeorological forecasting system is necessary in this region. The goals for the hydrometeorological modeling component were 1) to simulate a realistic hydrologic response for the headwater basins of the Carcarañá, 2) to provide a methodology to realistically hindcast and forecast extreme hydrometeorological events in the region, and 3) to investigate the added value of an advanced regional atmospheric data assimilation technique on hydrologic prediction.

This study provides an observation and modeling-based study of a hydrometeorological flash flood event caused by a severe convective storm during the early morning of 27 November 2018 in the Rio Tercero headwater subbasin of the Carcarañá watershed. It is organized as follows: in section 2, the principal characteristics of the region and the observed data are presented. The model specifications, statistical methods, and the experimental design are also discussed in this section. In section 3, the results are discussed, and finally, in section 4, the conclusions are summarized.

2. Data and methods

a. Study region and its characteristics

Our study region is the Rio Tercero river basin, in the northern headwaters of the Carcarañá basin (3184 km^2; Fig. 1a) in Argentina; it ranges in elevation from 371 to 2593 m (Fig. 1b). This basin drains east from the SDC mountain range, toward the plains. The streamflow measurement locations are Santa Rosa de Calamuchita (32.06°S, 64.55°W), Quillinzo (32.28°S, 64.53°W), and La Cruz (32.29°S, 64.48°W) (Fig. 1b). Spatial variations in climatic conditions resulting from elevation gradients lead to different vegetation types in this watershed. Figure 1c depicts the wide range of ecosystems in the region including mixed shrubland/grassland, croplands and sparsely vegetated regions. Figure 1d illustrates the surface soil texture classification with dominant soil classes as loamy sand and sandy loam, followed by silt loam and loam. Both vegetation and soil map are obtained from Instituto Nacional de Tecnología Agropecuaria (INTA). The climate is semiarid with mean annual precipitation ranging between 500 and 700 mm, of which more than 50% falls during summer (December–February). MCSs play an important role in extreme precipitation in this river basin. Analysis of Tropical Rainfall Measuring Mission (TRMM 2011) data over the period 2000–09 using the methodology of Rasmussen et al. (2016), reveals that around 46% of September–February extreme rainfall (over 99th percentile) over the larger Carcarañá watershed comes from MCS events (Fig. 2). Given that this headwater region is critical for tourism and electricity supply through hydroelectric power, it is necessary to analyze and model these extreme rainfall events.

b. Observed data

1) Observations from RELAMPAGO

Precipitation and streamflow data were collected during RELAMPAGO project. Precipitation data from 13 rain gauges [nine of them maintained by Ministerio de Agricultura y Ganaderia from the Córdoba Province or MAGYA and four from National Center for Atmospheric Research (NCAR)

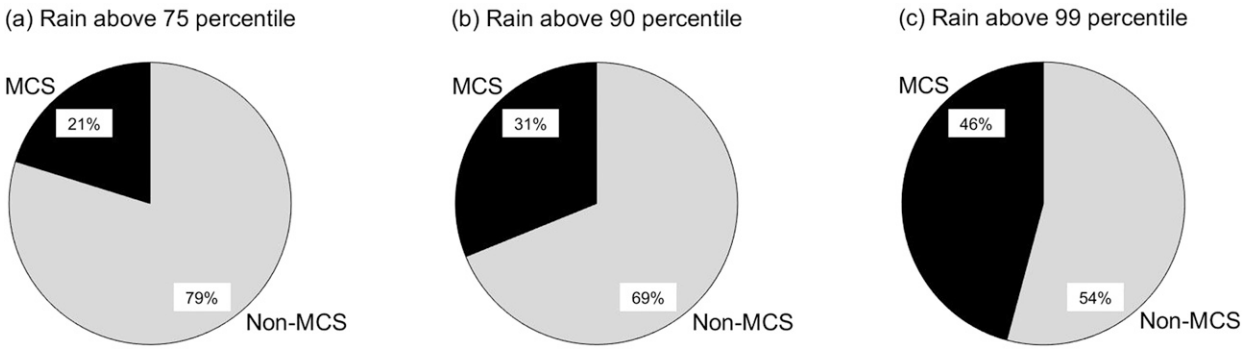

FIG. 2. Importance of MCS events in extreme precipitation in the watershed (precipitation climatology analyzed with TRMM data over the period 2000–09).

Research Application Laboratory (RAL)] were available during the IOP (see Fig. S1 in the online supplemental material for locations). To obtain continuous stage data in the rivers, the Ministerio de Servicios Públicos from the Córdoba Province installed three Bertschi 26G RD92 radar sensors within the Tercero Basin with a profiling range between 0.5 and 30 m and a measuring accuracy of ±3 mm (manufacturer specified nominal accuracy; actual uncertainties could be higher due to water surface fluctuations induced mainly by turbulence). The measurement interval was set at 10 min. The advantage of using radars is that the signal is generally immune to weather conditions, such as snow and rain (Sauer and Turnipseed 2010). These sensors remain installed even after the RELAMPAGO campaign, ensuring continuity of the measurements.

In low-flow conditions, we used YSI/SonTek RiverSurveyor S5 3-MHz ADCP with four-beam Janus configurations (similar to Herrero et al. 2018) to measure streamflow in the three rivers. An ADCP is a hydro-acoustic current meter used to measure water current velocities over a depth range, using the Doppler effect of sound waves scattered back from particles within the water column. The cell size is selected automatically from 0.02 to 0.5 m according to the water velocity and depth (Herrero et al. 2018). Following the methods of Mueller et al. (2013), a minimum of four transects (>12 min of measurement) were made in each cross section of each tributary to obtain mean discharge data. ADCP is the most accurate, recognized, and applied velocimetry technique in river and channels.

During high-flow conditions, due to the sudden nature of flash floods in the mountainous rivers of the province, flow velocities and floating river debris endanger the ADCP instruments and operators. Members of our team have been working with the U.S. Geological Survey (USGS) to improve the LSPIV techniques used in high-flow cases (Patalano et al. 2017). LSPIV has been used for water-surface velocity estimation and discharge measurements in rivers (Muste et al. 2008; Le Coz et al. 2014; Patalano et al. 2017). The method uses results from image velocity processing by solving the homography matrix that is the reduced form of the camera matrix assuming that all control points and the free surface are in the same plane [see Patalano et al. (2017) for detailed methodology]. When compared to the accurate measurements of ADCP, the errors with LSPIV were found to range between 5% and 10%. One reason for these errors was likely the conversion of surface discharge (measured) to actual discharge using a conversion factor.

We measured streamflow at the three locations shown in Fig. 1b to create the stage–discharge curves in these rivers and have continuous streamflow measurement (from stage values) thereafter. Furthermore, with the knowledge of the flows in these three rivers, total water coming into the Rio Tercero Dam (Fig. 1c) can be estimated for water management purposes.

During the RELAMPAGO IOP, daily weather forecasts allowed the hydrometeorology team enough time to deploy instrumentation and personnel to the basins with highest probability of intense precipitation. As an example, if the highest probability of precipitation was in the most remote stream gauging station, our team prepared for an overnight stay closer to the station because we would not have enough time to deploy if we remained in the operations center. In this way, we were able to construct the stage–discharge curves (Fig. 3) for the three basins during the IOP, despite the rapid response time in these rivers.

2) REMOTE SENSING PRODUCTS (IMERG)

The Integrated Multisatellite Retrievals for Global Precipitation Measurement (IMERG) products provide quasi-global (60°N–60°S) precipitation estimates passive microwave (PMW) and infrared (IR) satellites of the GPM constellation. These are level-3, 30-min gridded precipitation products at 0.1° × 0.1°, and calibrated by gauge analysis of the Global Precipitation Climatology Centre (GPCC; Schneider et al. 2011). The IMERG products are available in the form of near-real-time (NRT) data (i.e., IMERG-Early and -Late, IMERG-E and IMERG-L hereafter) and in the form of post-real-time research data (i.e., IMERG-Final, IMERG-F hereafter). The National Aeronautics and Space Administration (NASA) runs the final IMERG cycle after receiving monthly rain gauge analysis to create IMERG-F. This product has latency of around 3 months. In this study all three IMERG products have been used as quantitative precipitation estimate for analyzing precipitation and forcing the hydrologic model. The IMERG precipitation product was interpolated to

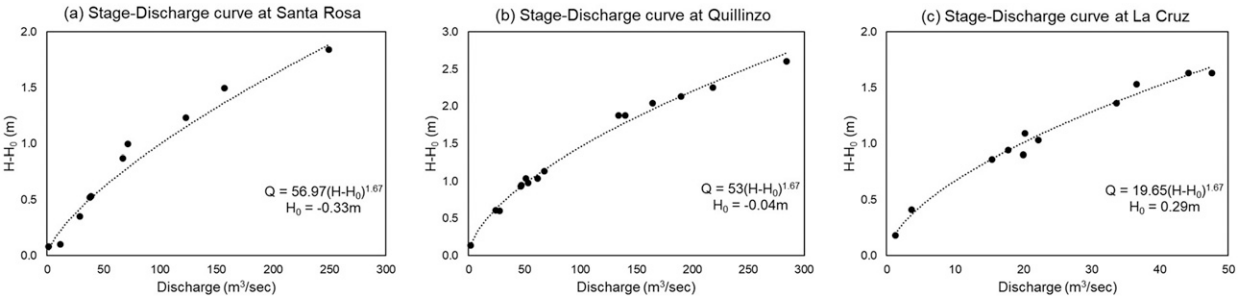

FIG. 3. Stage–discharge curves constructed in the three river locations Santa Rosa de Calamuchita, Quillinzo, and La Cruz during RELAMPAGO field campaign. Empirical equations of the curves are also indicated where H = stage measured (m), H_0 = water level for zero discharge (m), and Q = discharge ($m^3 s^{-1}$).

WRF-Hydro grid (1 km × 1 km) and used for the simulations IMERG-E–WRFHydro, IMERG-L–WRFHydro, and IMERG-F–WRFHydro (see Table 1).

3) ERA5 REANALYSIS DATA AND GFS DATA

ERA5 is the recent (2016) reanalysis data produced by the European Centre for Medium-Range Weather Forecasts (ECMWF) with a horizontal resolution of ~ 31 km (TL639 spectral grid) and 137 hybrid sigma–pressure levels in the vertical (with the top level located at 0.01 hPa, an altitude of about 80 km). ERA5 uses its 4DVAR data assimilation system at every 6 h in reanalysis mode. ''Surface'' or ''single level'' data are also available, containing 2D parameters such as precipitation, 2-m temperature, top-of-atmosphere radiation, and vertical integrals over the entire atmosphere. We retrieved the data at 0.25° × 0.25° horizontal resolution at all pressure levels and surface level. More detailed descriptions of the ECMWF reanalyses and their differences can be found in Dee et al. (2011) and Hersbach and Dee (2016). Recently ERA5 data have proven to be suitable for hydrologic application in Tarek et al. (2020). In this study, for the first time, we show the hydrologic application of dynamically downscaled ERA5 data [using the Weather Research and Forecasting (WRF) Model] in flash flood simulations (Table 1).

The Global Forecast System (GFS) is a weather forecast model produced by the National Centers for Environmental Prediction (NCEP) and extensively used for short to medium range meteorological forecast. GFS uses its Global Data Assimilation System (GDAS) only at the time of initialization and then runs in forecast mode [hybrid four-dimensional ensemble–variational formulation (hybrid 4DEnVar); Buehner et al. 2013]. Here we use GFS 3-hourly forecast at 0.25° × 0.25° resolution to force WRF. Notably, during the RELAMPAGO IOP, deployment decisions were made in part using convection-permitting GFS–WRF (WRF dynamically downscaled GFS data).

c. *Model description*

1) WRF

The meteorological modeling system used in this study is WRF, version 3.8.1 (Skamarock et al. 2008). The model domain includes the entire southern La Plata river basin (28°–37°S, 58°–76°W; Fig. S2). The domain of the meteorological model is set up at convection-permitting 3-km horizontal grid spacing, larger than the hydrological model domain, to capture the large-scale forcing and interactions. The convection-permitting modeling has the advantage of being able to accurately represent the characteristics of precipitation at event and climate scale (Prein et al. 2015; Pal et al. 2019). Some details of the configuration of the model are shown in Table S1. The physical parameterizations are the same as in previous convection-based studies in the region, which have provided a consistent representation of the temperature and precipitation (Mulholland et al. 2019) and also used for twice-daily operational forecasting during RELAMPAGO IOPs. We used different meteorological data as initial and boundary

TABLE 1. Experimental set up used in this study to evaluate the performance of different meteorological forcing data and models.

Hydrologic simulation name	Meteorological forcing	Precipitation forcing	Hydrologic model	Purpose
IMERG-E–WRFHydro	ERA5–WRF	IMERG-E	WRF-Hydro	NRT flood reconstruction
IMERG-L–WRFHydro	ERA5–WRF	IMERG-L		NRT flood reconstruction
IMERG-F–WRFHydro	ERA5–WRF	IMERG-F		Benchmark simulation, calibration of WRF-Hydro
ERA5–WRFHydro	ERA5–WRF	ERA5–WRF		Hindcast simulations, evaluating the capability of ERA5–WRF precipitation for hydrological applications
GFS–WRFHydro	GFS–WRF	GFS–WRF		Forecast simulations, evaluating the predictability of the event using GFS–WRF precipitation
LETKF–WRFHydro	GFS+GEFS–WRF	LETKF–WRF		Forecast simulations, evaluating the predictability of the event using LETKF–WRF ensemble precipitation

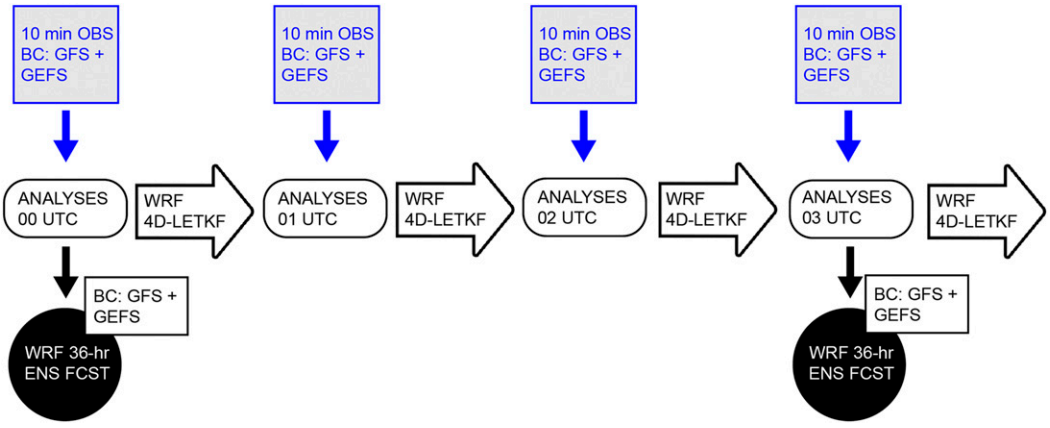

FIG. 4. LETKF–WRF flow diagram. An ensemble of analyses is computed hourly using the WRF Model coupled with a 4D-LETKF data assimilation technique. Every hour the observations (OBS) are assimilated separated into 10-min slots. The 36-h ensemble forecasts are computed only at 0000, 0300, 0600, 0900, 1200, 1500, 1800, and 2100 UTC. The boundary conditions (BC) are set using the GFS combined with the GEFS. See the text for a detailed description. ENS FCST = ensemble forecast.

conditions to force WRF (Table 1). For example, ERA5–WRF uses ERA5 data as forcing for WRF. Similarly, GFS–WRF uses GFS while local ensemble transform Kalman filter (LETKF)–WRF uses GFS+GEFS (Global Ensemble Forecast System) for the boundary conditions (see Table 1). WRF generated precipitation was interpolated to WRF-Hydro grid (1 km) to provide a 48-h streamflow forecast, with WRF initialization at 0000 UTC 26 November 2018.

2) LETKF–WRF

The LETKF–WRF is the regional ensemble-based data assimilation system computed in real time during the campaign. This system [named RELAMPAGO Rapid Refresh (RRR)] was jointly developed by the Argentinian National Meteorological Service and the Department of Atmospheric Sciences of University of Illinois. The simulations were run using the NCAR supercomputer Cheyenne resources (CISL 2019). WRF version 3.9.1.1 with a 10-km horizontal resolution was used, coupled with a 4D local ensemble transform Kalman filter (4D-LETKF) (Hunt et al. 2007; Miyoshi and Kunii 2011) data assimilation technique (hereafter LETKF–WRF). A 60-member ensemble was constructed using nine combinations of cumulus and planetary boundary layer parameterizations, and the 20-member GEFS recentered around the 0.25° deterministic GFS as boundary conditions. 60-member ensemble precipitation forecasts obtained from LETKF–WRF is used for LETKF–WRF-Hydro simulation (Table 1). A flow diagram of the system is shown in Fig. 4. An ensemble of hourly analyses is obtained through a 4D-LETKF implementation which assimilates the observations from the previous hour distributed in 10-min slots. In addition, 36-h ensemble forecasts are computed every 3 h, i.e., eight times a day. The sources of the observations assimilated are C-band Argentinian radar network, *GOES-16*-derived motion winds, Atmospheric Infrared Sounder (AIRS) retrievals, automatic and conventional surface weather stations, airplanes, radiosondes, ships, and buoys. For example, the distribution of the observations assimilated for the 1200 UTC 26 November 2018 analyses is shown in Fig. 5. The LETKF–WRF system was started at 0100 UTC 5 November 2018 and continuously run until 1200 UTC 19 December 2018. A detailed description of a similar regional data assimilation technique can be found in Dillon et al. (2016). For this work, 12- and 36-h ensemble forecasts initialized at 0000 and 1200 UTC 26 November, respectively, were used.

3) WRF-HYDRO

WRF-Hydro 5.0.3 (Gochis et al. 2018) is a parallelized distributed hydrologic model. In the case of our study, it has the advantage that it can either be forced offline using prescribed atmospheric forcing variables or coupled seamlessly to the Advanced Research version of WRF (WRF-ARW as dynamical core). Atmospheric forcing data needed to execute WRF-Hydro include incoming shortwave radiation, incoming longwave radiation, specific humidity, air temperature, surface pressure, and near surface wind (both u and v components). In this study, WRF-Hydro 5.0.3 is configured in its uncoupled mode, so the hydrological model obtains only atmospheric input forcing from the atmospheric model. Noah multiparameterized land surface model (Noah-MP LSM) is the land surface model (Niu et al. 2011) used in WRF and uncoupled WRF-Hydro. The WRF-Hydro modeling system was set up using multiple grid structures in the basin, such that the Noah-MP LSM was operated at 1-km horizontal grid spacing with an additional representation of overland flow, along with channel routing on a nested 100-m grid (e.g., Gochis and Chen 2003; Gochis et al. 2018) to accurately represent the river network in this complex terrain. Noah-MP consists of a four-layer soil model (10-, 30-, 60-, and 100-cm thickness). The fine-resolution grid of 100 m further redistributes terrestrial moisture. Subsequently, surface water head and soil moisture content for each soil layer is aggregated and updated in the coarse Noah-MP LSM grid. Calculation of surface runoff uses infiltration capacity excess. Here infiltration capacity excess in the 1D column model domain is allowed to

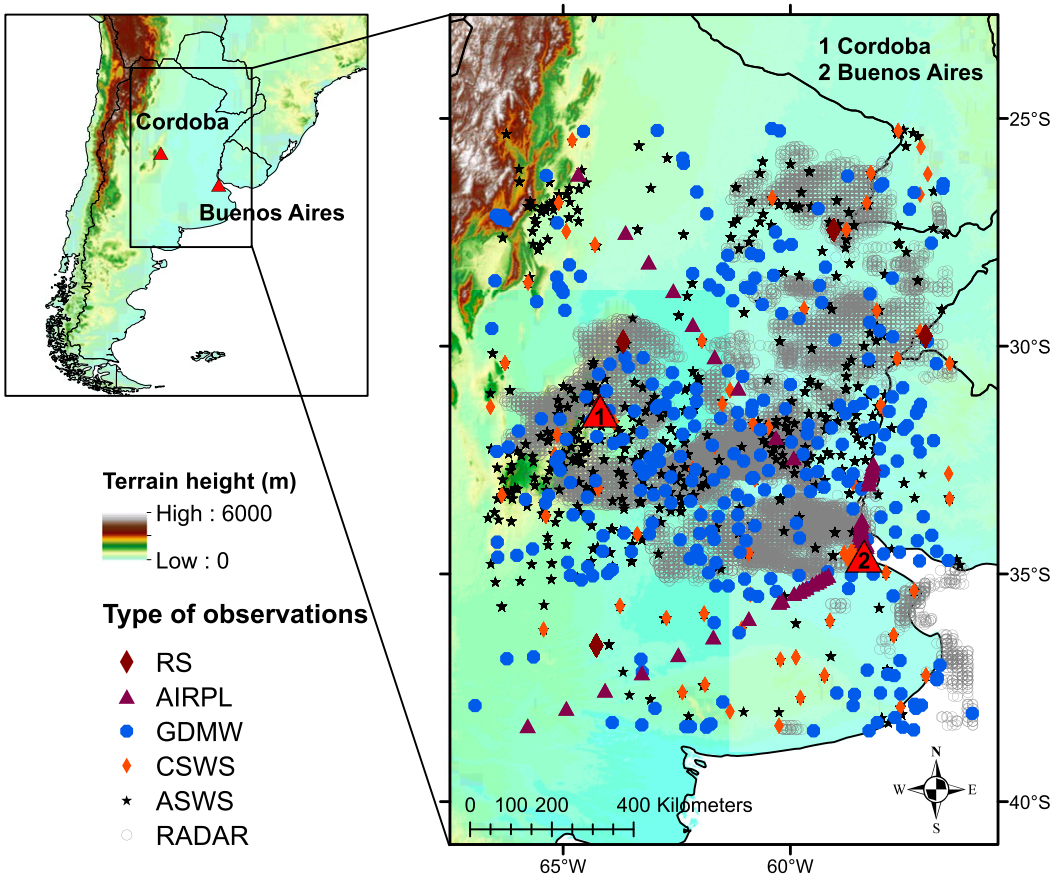

FIG. 5. Distribution of the different types of assimilated observations for the 1200 UTC 26 Nov 2018 ensemble analyses. Following are the total amount of observations from each type indicated within brackets. RS = radiosondes (597), AIRPL = aircraft data (120), GDMW = *GOES-16*-derived motion winds (572), CSWS = conventional surface weather stations (635), ASWS = automatic surface weather stations (8914), RADAR = Argentinian C-band radars (29232). The elevation (m) is shaded.

remain within the model domain as "ponded water," which is subsequently available for lateral redistribution. See Yucel et al. (2015) and Gochis et al. (2018) for more detailed information about WRF-Hydro. Initial soil moisture condition for WRF-Hydro was derived from corresponding forcing data for WRF. The WRF-Hydro system includes various predefined hydrological parameters. Previous studies have recommended calibrating several sensitive parameters, especially those controlling the total water volume and the temporal distribution of streamflow, to improve model performance in terms of the volume of discharge and shape of the hydrograph (Yucel et al. 2015; Naabil et al. 2017). Parameters found most important for this study are infiltration factor (REFKDT) and channel Manning roughness or Manning's *N*. The other parameters (such as soil and vegetation parameters) are taken as default WRF-Hydro configuration (Gochis et al. 2018) and kept constant throughout the simulations. REFKDT controls the rate of surface infiltration at each time step. Higher REFKDT values result in lower simulated hydrograph volume at an unsaturated soil condition.

We calibrated WRF-Hydro using IMERG-F because it is a bias-corrected gridded remotely sensed product that provided an adequate representation of the area-averaged precipitation when compared to rain gauge data. We did not use rain gauges directly because they are not uniformly distributed throughout the watershed, and we would lose spatial detail in the gridding process. Also, some of the rain gauges were withdrawn after RELAMPAGO. Within WRF-Hydro, REFKDT is calibrated in this study by manually varying its value between 0.02 and 0.5 to get an optimum value of 0.3 (Table 2). Another important parameter in WRF-Hydro, deciding the shape of hydrograph, is Manning's *N*. These depend on stream order and are controlled by the scaling factor MannN in WRF-Hydro (Gochis et al. 2018). A manual calibration was carried out in this study by multiplying the Manning's roughness values by scaling factors of 0.5, 1 (default), 1.4, and 2. Optimum value of MannN was found to be 1.4 (Table 2), and corresponding roughness coefficients ranging from 0.77 to 0.014 (Table 3). Calibration was performed based on the RMSE and NSE values (see Table 4) of streamflow following past literature (Nash and Sutcliffe 1970; Moriasi et al. 2007; Varlas et al. 2019; Furnari et al. 2020). The other parameters of WRF-Hydro, which were stated as sensitive in past studies, like surface retention depth (RETDEPRTFAC) or overland routing parameter

TABLE 2. Manual calibration of the two most sensitive parameters of WRF-Hydro, infiltration parameter (REFKDT) and channel roughness parameter (MannN), based on precipitation forcing from IMERG.

		RMSE ($m^3 s^{-1}$)			NSE		
	Value	Santa Rosa	Quillinzo	La Cruz	Santa Rosa	Quillinzo	La Cruz
REFKDT (MannN = 1) (infiltration parameter)	0.02	81.78	78.96	43.32	0.22	0.31	0.05
	0.1	76.24	70.47	32.46	0.24	0.33	0.07
	0.3	67.15	65.11	21.55	0.25	0.56	0.11
	0.5	76.29	70.05	45.86	0.25	0.55	0.11
MannN (REFKDT=0.3) (channel roughness parameter)	0.5	81.22	75.16	35.77	0.15	0.45	0.19
	1	67.15	65.11	21.58	0.25	0.56	0.11
	1.4	58.97	62.55	15.95	0.56	0.62	0.60
	2	88.92	81.29	41.28	0.34	0.56	0.19

(OVROUGHTFRA) were not found to be sensitive for this short simulation. The optimum values of REFKDT and MannN obtained from manual calibration with IMERG-F data were applied to other forcing datasets. We acknowledge that with better estimates of channel geometry, roughness, and soil properties, the modeling can be significantly improved.

d. Experimental design

In summary, we designed the simulations in such a way that the capability of the meteorological and hydrological models can be tested (Table 1). We use 1) IMERG-E and IMERG-L as NRT flood reconstruction, 2) IMERG-F as a benchmark for spatially distributed precipitation and WRF-Hydro calibration, 3) ERA5–WRF in hindcast mode with continuous assimilation to investigate the usage of the state-of-the-art ERA5 reanalyses for a posteriori hydrometeorological application, 4) GFS–WRF as a deterministic forecast to be used in an operational context as it uses assimilation only for initial conditions, and 5) ensemble precipitation forecast from LETKF–WRF initialized with regional-scale data assimilation, which provides the opportunity to evaluate the applicability of an ensemble-based forecast with assimilation, as compared to a deterministic one.

e. Statistical metrics and methods

We use different objective metrics to evaluate the deterministic and ensemble atmospheric forecasts, and streamflow simulations (Table 4). In addition to the metrics listed in the table, we use area under relative operating characteristics (AROC) curve (Wilks 2011) value to show the skill of forecasts discriminating between the occurrence and nonoccurrence of precipitation. A perfect forecast system is represented by AROC equal to 1, while an AROC below 0.5 indicates no skill. We also use rank histograms to evaluate whether the collection of ensemble forecasts satisfy the consistency condition (Wilks 2011). We use the Thiessen polygon method to assign areal significance to gauge rainfall estimates. It is a method where perpendicular bisectors are constructed to the lines joining each measuring station with those immediately surrounding it. These bisectors form a series of polygons, each polygon containing one station. The value of precipitation measured at a station is assigned to the whole area covered by the enclosing polygon (American Meteorological Society 2020).

3. Results and discussion

a. Development and synoptic environment

During 26–27 November 2018, deep convection repeatedly formed over the southern Sierras, and organized into an MCS, leading to significant flooding and an important hydrological event for the RELAMPAGO IOP. GOES IR imagery, as created by NCAR Earth Observing Laboratory (EOL), was made available during RELAMPAGO (Fig. 6). At 0000 UTC

TABLE 3. Default channel parameter table (MannN = 1) and the values used in this study (with MannN = 1.4) in WRF-Hydro. Bw = channel bottom width (m), HLINK = initial depth of channel water (m), ChSSlp = channel slope, and Manning's N = actual roughness coefficients corresponding to the stream order. Lower stream order is associated with upstream area.

Stream order	Bw (m)	HLINK (m)	ChSSlp (rise/run)	Default Manning's N	Manning's N used (scaling factor 1.4)
1	1.5	0.02	3	0.55	0.77
2	3	0.02	1	0.35	0.49
3	5	0.02	0.5	0.15	0.21
4	10	0.03	0.18	0.1	0.14
5	20	0.03	0.05	0.07	0.10
6	40	0.03	0.05	0.05	0.07
7	60	0.03	0.05	0.04	0.06
8	70	0.1	0.05	0.03	0.04
9	80	0.3	0.05	0.02	0.03
10	100	0.3	0.05	0.01	0.01

TABLE 4. List of statistical metrics used for verification of precipitation and streamflow simulations. Here, P^i_{model} = model-simulated precipitation at ith hour, P^i_{obs} = observed IMERG-F precipitation at ith hour, n = number of hours in consideration, a = hits, b = false alarms, c = misses, and d = correct rejection of the 2 × 2 contingency table (Wilks 2011) for detection of precipitation ≥1 mm; Q_{obs} = observed streamflow and Q_{model} = WRF-Hydro simulated streamflow.

	Statistical metric	Equation	Perfect value	Unit	Purpose
Precipitation verification	Correlation coefficient (CC)	$\frac{\text{covariance}(P_{\text{model}}, P_{\text{obs}})}{\sigma P_{\text{model}} \sigma P_{\text{obs}}}$	1		Quantify agreement with observations
	Mean error (ME)	$\frac{1}{n}\sum_{i=1}^{n}(P^i_{\text{model}} - P^i_{\text{obs}})$	0	mm h^{-1}	Quantify deviation from observations
	Mean square error (MSE)	$\frac{1}{n}\sum_{i=1}^{n}(P^i_{\text{model}} - P^i_{\text{obs}})^2$	0	mm^2 h^{-2}	Quantify deviation from observations
	Root-mean-square error (RMSE)	$\sqrt{\frac{1}{n}\sum_{i=1}^{n}(P^i_{\text{model}} - P^i_{\text{obs}})^2}$	0	mm	Quantify deviation from observations
	Probability of detection (POD)	$\frac{b}{b+d}$	1		Quantify precipitation detection capability
	False alarm ratio (FAR)	$\frac{b}{a+b}$	0		Quantify precipitation detection capability
	Critical success index (CSI)	$\frac{a}{a+b+c}$	1		Quantify precipitation detection capability
Streamflow verification	Correlation coefficient (R)	$\frac{\text{covariance}(Q_{\text{model}}, Q_{\text{obs}})}{\sigma Q_{\text{model}} \sigma Q_{\text{obs}}}$	1		Quantify agreement with observations
	Root-mean-square error (RMSE)	$\sqrt{\frac{1}{n}\sum_{i=1}^{n}(Q^i_{\text{model}} - Q^i_{\text{obs}})^2}$	0	m^3 s^{-1}	Quantify deviation from observations
	Nash–Sutcliffe efficiency (NSE)	$1 - \frac{\sum_{i=1}^{n}(Q^i_{\text{model}} - Q^i_{\text{obs}})^2}{\sum_{i=1}^{n}(Q^i_{\text{model}} - \overline{Q^i_{\text{obs}}})^2}$	1		Quantify agreement with observations

27 November convection initiated over the high terrain south-southwest of Córdoba (Fig. 6a). Then it grew and moved east (Fig. 6b). At 0315 UTC (Fig. S3), growth was primarily by backbuilding and the system started moving off the terrain (Fig. 6c). Later it became more stratiform in nature (Fig. 6d). The storm continued affecting the basin until ~1200 UTC or 0900 local time (LT; corresponds to UTC − 3 h) and then it moved farther northeast (Fig. S3). We analyze the synoptic conditions prevailing at the time of the event based on ERA5 hourly data (Fig. 7). Westerlies aloft (250 mb; 1 mb = 1 hPa) were driven by east–west jet streaks over southern South America (~35°S; Fig. 7a). The 500-mb geopotential height contours reveal a shortwave trough located off the Chilean coast (Fig. 7b). This acted as a large-scale forcing mechanism for deep convection. The 500-mb westerly winds (Fig. 7b) imposed a cap on the lower level and helped in building of instability in the region. In addition, integrated vapor transport (shaded in Fig. 7b) reveals the dominant southward moisture transport at (>300 kg m^{-1} s^{-1}) ~ 30°S, which was supportive of the extreme rainfall event. Figure 7c indicates the southward moisture advection by the 850-mb winds which in turn increases the specific humidity near the basin. This is a signature of SALLJ carrying moisture from lower latitudes south (Salio et al. 2002, 2007). Finally, Fig. 7d confirms the warm air advection at ~30°S at the lower level. To understand the role of lower-level moisture advection during this event we plot a Hovmöller diagram of meridional wind (V wind; Fig. 8a) and moisture flux due to meridional wind (Vq; Fig. 8b). It is clear that prior to the event ~0000 UTC 27 November, there is a strengthening of northerly SALLJ (deep purple shading) at ~850 mb carrying moisture southward. We see a reversal of lower-level wind direction after the event ~0000 UTC 28 November. These mesoscale and synoptic-scale forcing help build the instability required for the deep moist convection. Sounding taken at Córdoba (Fig. 9) prior to the event indicates a high MUCAPE and minimum CIN along with the very moist lower level (from the surface to 850 mb). The northerly low-level wind is also prominent in this figure. In summary, a northerly low-level jet advected warm and moist air while synoptic and thermodynamic conditions were favorable for convection.

b. *Analysis of precipitation*

As mentioned in section 1, accurate representation of spatial distribution and timing of precipitation is very important for flash flood forecasting. In this section we analyze the available precipitation products during the event. The time series correlation between rain gauges and IMERG-F was found to be 0.81, and the spatial pattern was well captured, with more precipitation toward southern part of the basin and less precipitation toward northern part (see Fig. 12 and Fig. S4). The slight discrepancies between ground-based observations and satellite estimations can be attributed to nonuniform distribution of rain gauges over the basin and inaccuracies in the remotely sensed precipitation. Thus, we compare other

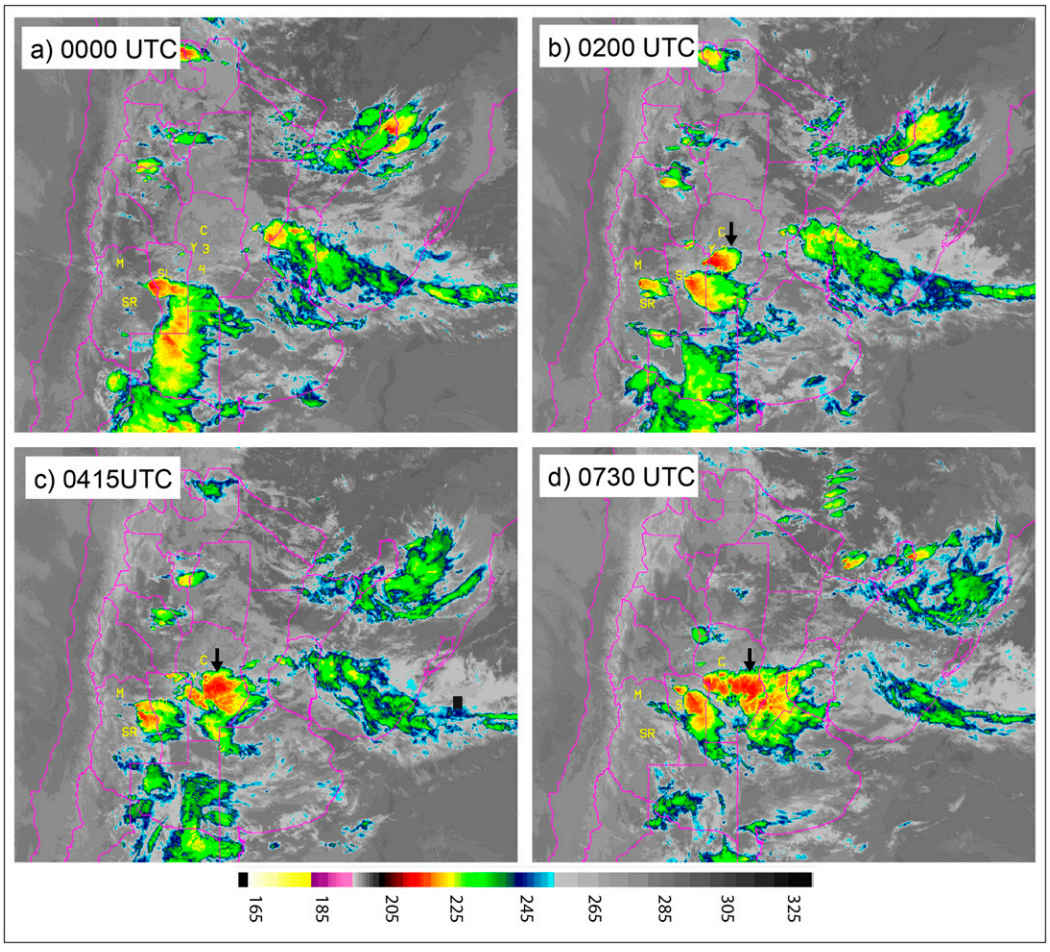

FIG. 6. (a)–(d) Evolution of the storm during RELAMPAGO as seen by GOES IR imagery [colors represent brightness temperature (K)]. The times of snapshots are indicated. The black arrow in (b), (c), and (d) points at the storm that affected the basin. The images were processed by NCAR EOL during the RELAMPAGO field campaign. C = Córdoba, Y = Yacanto, M = Mendoza, SR = Santa Rosa, SL = San Luis.

gridded precipitation products (used as forcing for the hydrologic model) with IMERG-F as our benchmark in this paper.

1) SPATIAL ANALYSIS

The MCS generated from the elevated convection near SDC resulted in heavy precipitation over the basin starting on 26 November at 2000 LT and lasting about 10 h. The period of analysis was from 0000 UTC 26 November 2018 to 0000 UTC 28 November 2018 (48 h) to capture the full extent of the event. Figure 10 shows the hourly averaged rainfall from IMERG-E, IMERG-L, IMERG-F, ERA5–WRF, GFS–WRF, and LETKF–WRF for day 1 (0000 UTC 26 November–0000 UTC 27 November) and day 2 (0000 UTC 27 November–0000 UTC 28 November) of the event. Total accumulated precipitation during the event was >120 mm in some southern parts of the watershed. IMERG-E (Figs. 10a,g) and IMERG-L (Figs. 10b,h) overestimated the precipitation when compared with IMERG-F (Figs. 10c,i), especially on day 2. ERA5–WRF (Figs. 10d,j) showed similar intensity and spatial pattern of precipitation with IMERG-F. In terms of statistical metrics, ERA5–WRF had high CC (>0.7, Fig. 11a) and low RMSE (Fig. 11d) on the north and west, along with moderate CC (0.5–0.7, Fig. 11d) and RMSE south of the basin. GFS–WRF, on the other hand, failed to represent the spatial pattern of rainfall (Fig. 10e) and predicted higher rainfall west and southern part of the watershed. This is reflected in the low CC (<0.4, Fig. 11b) and high RMSE (Fig. 11e) values. The timing of the major precipitation event was also not captured in GFS–WRF, which is evident from Figs. 10e and 10k. These figures indicate that GFS–WRF significantly overestimated the rainfall over the basin during the first day and underestimated during the second day. In particular, GFS–WRF predicted more than 4 mm h^{-1} rainfall between 0600 and 1000 LT 26 November 2018, which is an overestimation of 2.5–3 mm h^{-1} (80%–100%) (Figs. 12a,b). Overall, 48-h accumulated precipitation at 0000 UTC 28 November is greater than 100 mm in the southwestern region, and the bias is less in ERA5–WRF than in GFS–WRF when compared with IMERG-F. The spatial pattern and timing of precipitation is significantly improved in LETKF–WRF (ensemble median, Figs. 10f

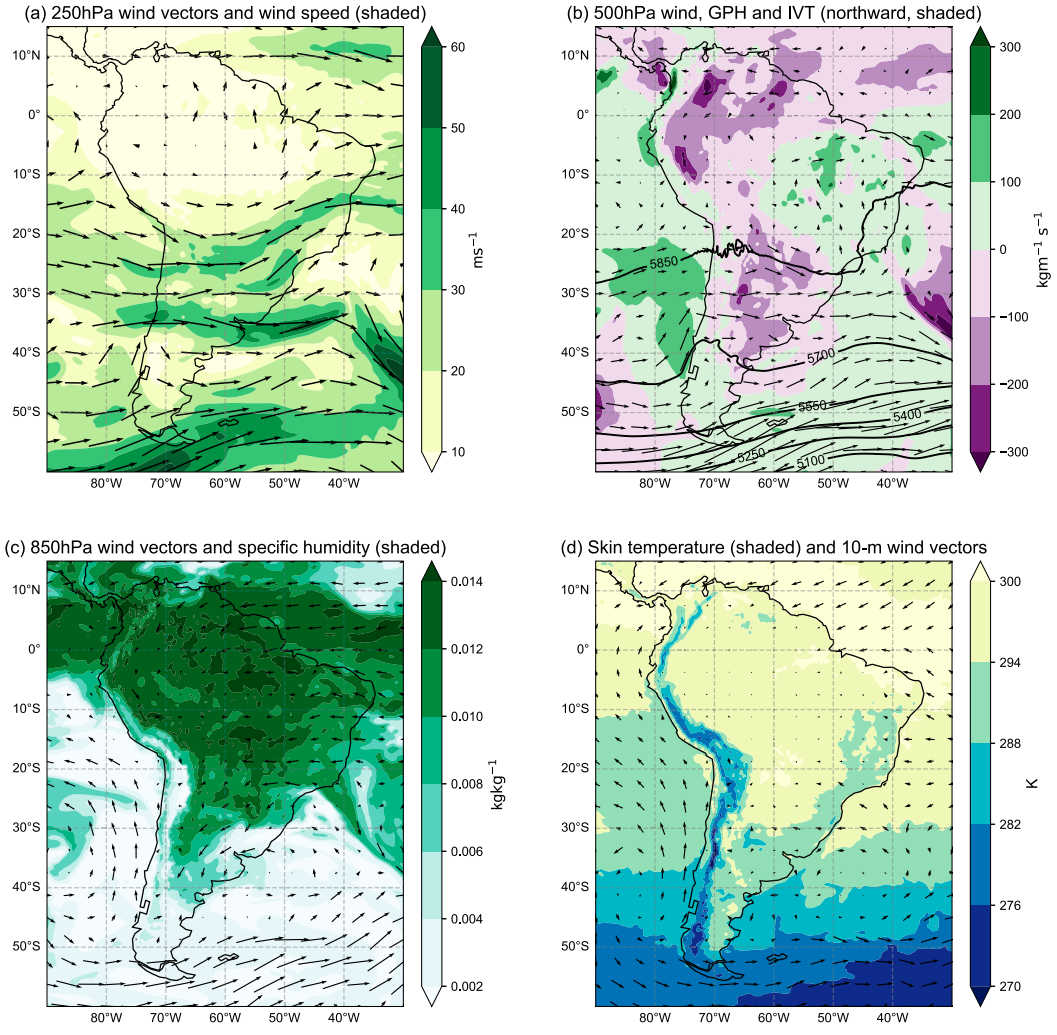

FIG. 7. Synoptic-scale conditions prevailing prior to the event (27 Nov 0000 UTC) from ERA5. (a) The 250-mb geopotential height showing an east–west jet streak over southern South America and westerlies aloft. (b) The 500-mb map reveals a slow-moving shortwave trough situated immediately offshore along the Chilean coast. Integrated vapor transport (IVT) indicates the southward moisture transport having a peak at the region of concern (30°S). (c) Northerly winds and moisture at 850 mb reveal the southward intrusion of moisture at lower level. (d) The temperature at the surface reveals the warming of surface right before the event.

and 10l) compared to GFS–WRF in terms of higher CC (>0.5 all over the basin) and lower RMSE (except northeast part).

In addition to the continuous metrics (CC and RMSE), we also evaluate ERA5–WRF, GFS–WRF, and LETKF–WRF (ensemble median) against IMERG-F using contingency statistical metrics (POD, FAR, and CSI, Fig. 11). POD (Figs. 11g–i) is in the range of 0.3–0.5 for ERA5–WRF and GFS–WRF with some higher values (>0.7) in the north for ERA5–WRF. LETKF–WRF achieves POD values 0.5–0.7 throughout the basin with higher values toward the north. FAR (Figs. 11j–l) is significantly high in GFS–WRF (>0.5) and eastern part of the basin in ERA5–WRF. Low FAR values (<0.3) are found throughout the basin for LETKF–WRF. In terms of CSI (Figs. 11m–o), LETKF–WRF achieves the highest values (0.3–0.5), while ERA5–WRF and GFS–WRF has lower values (<0.3) with the exception of high values in the north (>0.5) for ERA5–WRF. Overall, LETKF–WRF showed better performance than ERA5–WRF and GFS–WRF in terms of CC, POD, FAR, and CSI. GFS–WRF performed poorly, particularly in terms of FAR.

2) TEMPORAL ANALYSIS

Area average (over the basin in Fig. 1b) time series of precipitation (Figs. 12a,b) show that IMERG-E and IMERG-L overestimate the 48-h accumulated precipitation by 20–30 mm with slightly lower bias in IMERG-L. ERA5–WRF underestimates (negative ME, Fig. 13a) precipitation when compared to IMERG-F. Figure 12a indicates that precipitation on 26 November was overestimated in GFS–WRF and precipitation of 27 November was underestimated (also see ME

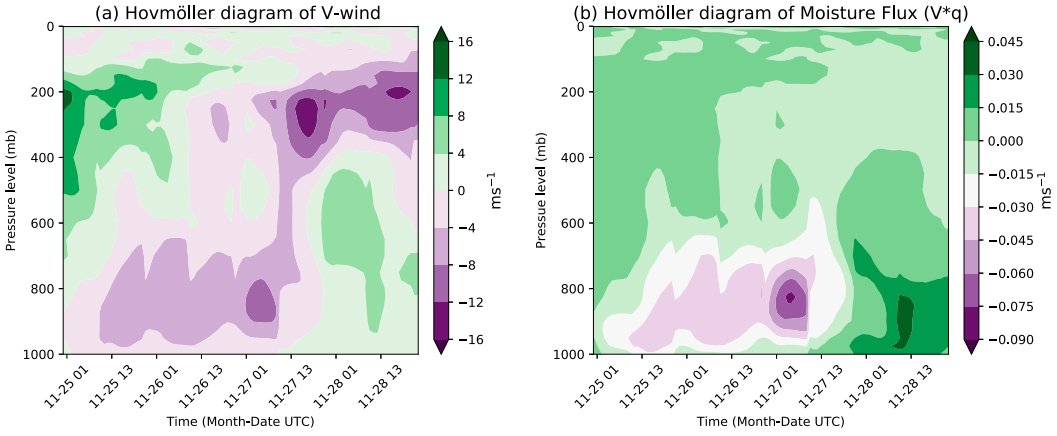

FIG. 8. Hovmöller diagram of (a) V wind and (b) moisture flux (Vq) from two days prior to the event through 1 day after the event. The values are averaged over the region from 30°N, 65°W to 35°N, 60°W. Negative values represent southward advection.

estimates in Fig. 13a). However, 48-h accumulated precipitation predicted by GFS–WRF at 0000 UTC 28 November is comparable to that of ERA5–WRF (Fig. 12b). In Fig. 12b, the brown line indicates median value of LETKF–WRF ensembles and orange shading shows the values lying within first and third quantile (interquartile range). The median value is close to the observed (both IMERG-F and rain gauge estimated) 48-h accumulation rainfall and the interquartile range of the ensemble spread encompasses the observations. Spaghetti plot of all ensemble members of LETKF–WRF (Fig. 13b) indicate lower

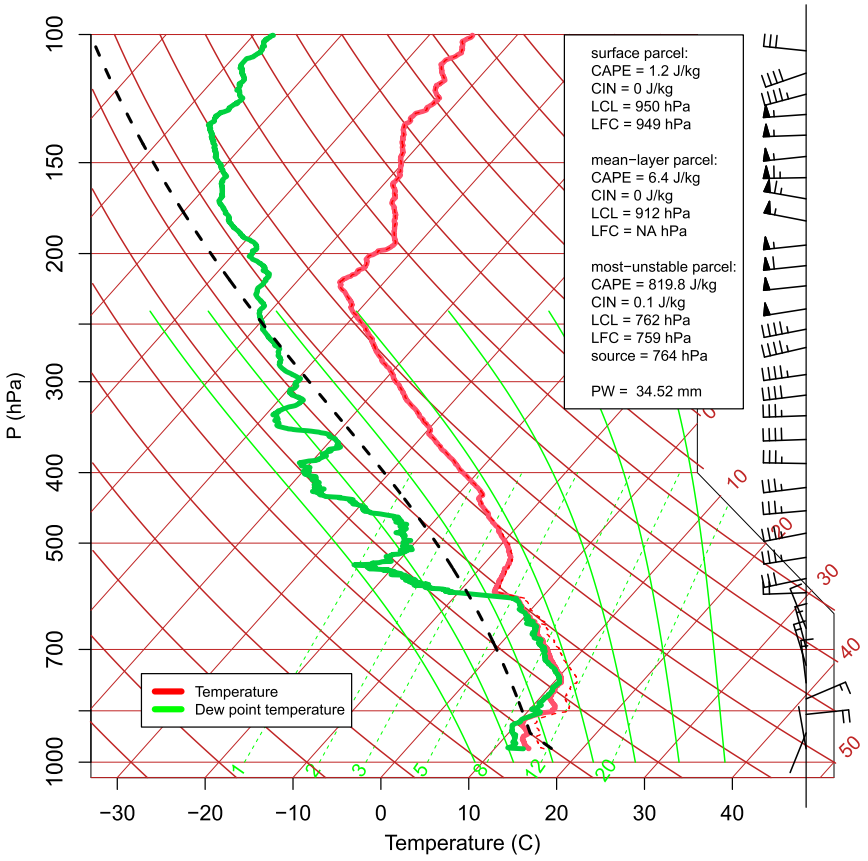

FIG. 9. Sounding taken from Córdoba (31.298°S, 64.212°W) at 2330 UTC 26 Nov 2018 during RELAMPAGO IOP. The dashed black line shows ascent of parcel with maximum equivalent potential temperature.

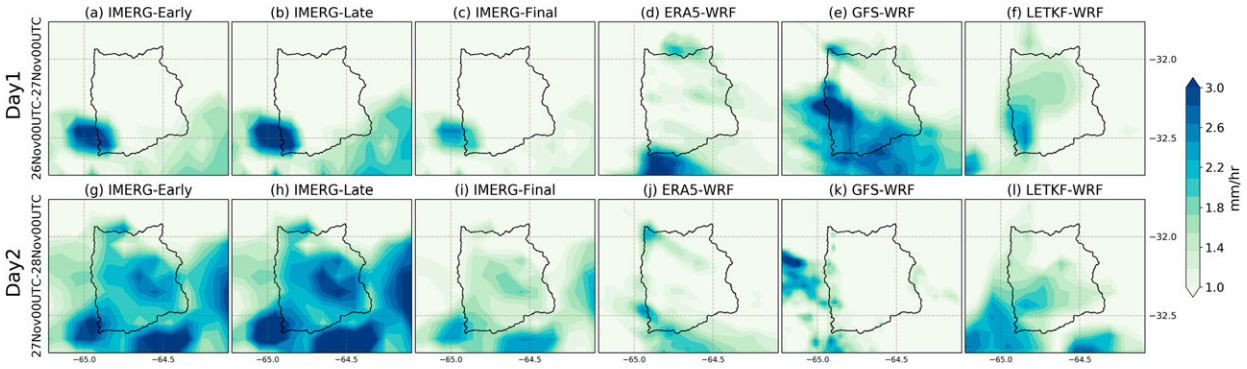

FIG. 10. Average rate of precipitation (mm h^{-1}) during day1 (0000 UTC 26 Nov–0000 UTC 27 Nov) and day 2 (0000 UTC 27 Nov–0000 UTC 28 Nov) as estimated by (a),(g) IMERG-E; (b),(h) IMERG-L; (c),(i) IMERG-F; (d),(j) ERA5–WRF; (e),(k) GFS–WRF; and (f),(l) LETKF–WRF ensemble median.

ME and MSE when compared to ERA5–WRF and GFS–WRF. Figure 13c shows AROC values for different forecasts and it is seen that models have higher skill during day 1 and lower skill as time progresses. Only LETKF–WRF was able to improve the score during hours 24–35. In general, ERA5–WRF and LETKF–WRF showed higher skill than GFS–WRF throughout the simulation. In addition, a uniform rank histogram (Fig. 13d) confirms the consistency among model ensemble members of LETKF–WRF. Overall, LETKF–WRF performed better than ERA5–WRF and GFS–WRF in terms of ME, MSE and AROC values. Model skill decreases with lead time except improved AROC value of LETKF–WRF during precipitation of day 2.

Due to the fact that WRF model configuration was unaltered, the inconsistency between ERA5–WRF and GFS–WRF predicted precipitation can be attributed to the initial and boundary conditions. ERA5 includes observation using 4DVAR data assimilation every hour, whereas GFS uses a global data assimilation system only at the initial time step. Therefore, the atmospheric boundary conditions degrade with forecast lead time. On the other hand, the LETKF–WRF uses a combination of GFS and GEFS as boundary condition and the data assimilation technique incorporates observations from the previous hour distributed in 10-min slots [section 2c(2)]. In this case, atmospheric regional data assimilation was able to capture the local and remotely sensed precipitation pattern (Fig. 10 and Fig. 11). Also, ensemble-based forecasting gives us an opportunity to consider the uncertainty in the model runs.

c. *Hydrologic response: Analysis of streamflow*

The results in this section are obtained from the best hydrologic model parameter combination as discussed in section 2. Figures 14b–d shows simulated and observed streamflow in the three rivers. The maximum flow discharge (stage) observed at Quillinzo, La Cruz, and Santa Rosa was 370 $m^3 s^{-1}$ (3 m), 50 $m^3 s^{-1}$ (2.6 m), and 260 $m^3 s^{-1}$ (1.8 m) at 1000, 1400, and 1200 LT, respectively. The time to peak at these locations was 5–6 h depending on the river concerned. The peak flood response was fast and intense at Quillinzo, slightly slower but very intense in Santa Rosa and slow and muted in La Cruz (Figs. 14b–d, black lines). Figure 14a depicts the corresponding IMERG-F hourly basin-average precipitation. Statistical evaluation of WRF-Hydro simulated streamflow is presented in Table 5.

At Quillinzo (Fig. 14b), the timing of peak flood (1000 LT 27 November) was well captured by IMERG-F–WRFHydro, though the magnitude was lower by 50–70 $m^3 s^{-1}$ (R = 0.74, RMSE = 62.55 $m^3 s^{-1}$, NSE = 0.62). IMERG-E–WRFHydro and IMERG-L–WRFHydro overestimated the peak and simulated earlier than observation (R = 0.58, RMSE = 138.87, NSE = 0.15 for IMERG-E–WRFHydro and R = 0.73, RMSE = 95.93, NSE = 0.4 for IMERG-L–WRFHydro). ERA5–WRFHydro represents the magnitude well, but the peak time was delayed by 5 h. This simulation has lower values of R and NSE (0.53 and 0.39, respectively) than IMERG-F–WRFHydro. GFS–WRFHydro predicts a very early peak (previous day ~1800 LT) with similar magnitude. This results in negative R and NSE values with high RMSE (146.01 $m^3 s^{-1}$, Table 5). LETKF–WRFHydro ensemble median streamflow peak is 2 h earlier than observed. However, the actual peak was captured closely by some of the ensemble members and hence, the interquartile range of the ensemble spread is very close to the observed flow. The R, NSE, and RMSE values (0.64, 0.24, and 84.81 $m^3 s^{-1}$, respectively) of LETKF–WRFHydro ensemble median were better than the GFS–WRFHydro metrics.

At La Cruz (Fig. 14c), IMERG-E–WRFHydro and IMERG-L–WRFHydro significantly overestimate the peak amount with higher bias in the former (RMSE = 74.92 and 59.55 $m^3 s^{-1}$, respectively). Although the magnitudes of peak flood were overestimated by IMERG-F–WRFHydro slightly (RMSE = 15.95 $m^3 s^{-1}$), CC and NSE was high (0.91 and 0.6, respectively). GFS–WRFHydro predicted an earlier and higher intensity peak flow with low R and NSE values. LETKF–WRFHydro ensemble was able to reduce some of the extreme behavior from simulation and the median represents well the observed streamflow. The R and NSE values were improved to 0.77 and 0.43, respectively, with significant reduction in RMSE (8.98 $m^3 s^{-1}$).

At Santa Rosa (Fig. 14d), both IMERG-E–WRFHydro and IMERG-F–WRFHydro perform better than IMERG-F–WRFHydro in terms of peak timing but overestimated the

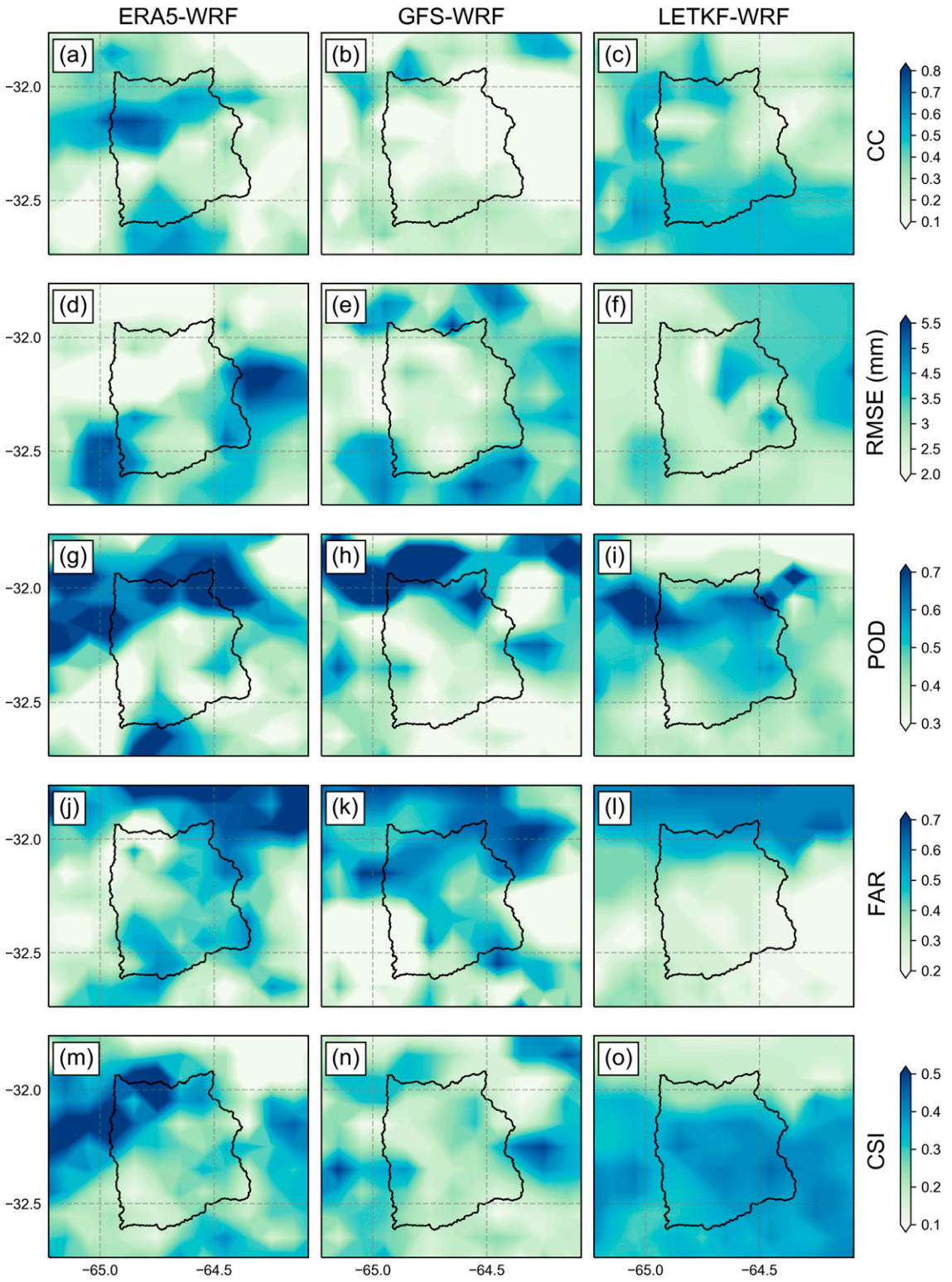

FIG. 11. Spatial distribution of the statistical metrics for the ERA5–WRF, GFS–WRF, and LETKF–WRF ensemble median precipitation at grid scale over Rio Tercero basin: (a)–(c) CC, (d)–(f) RMSE, (g)–(i) POD, (j)–(l) FAR, and (m)–(o) CSI. The time series of each grid cell during the full event (48 h) are used to calculate the metrics and plotted on map.

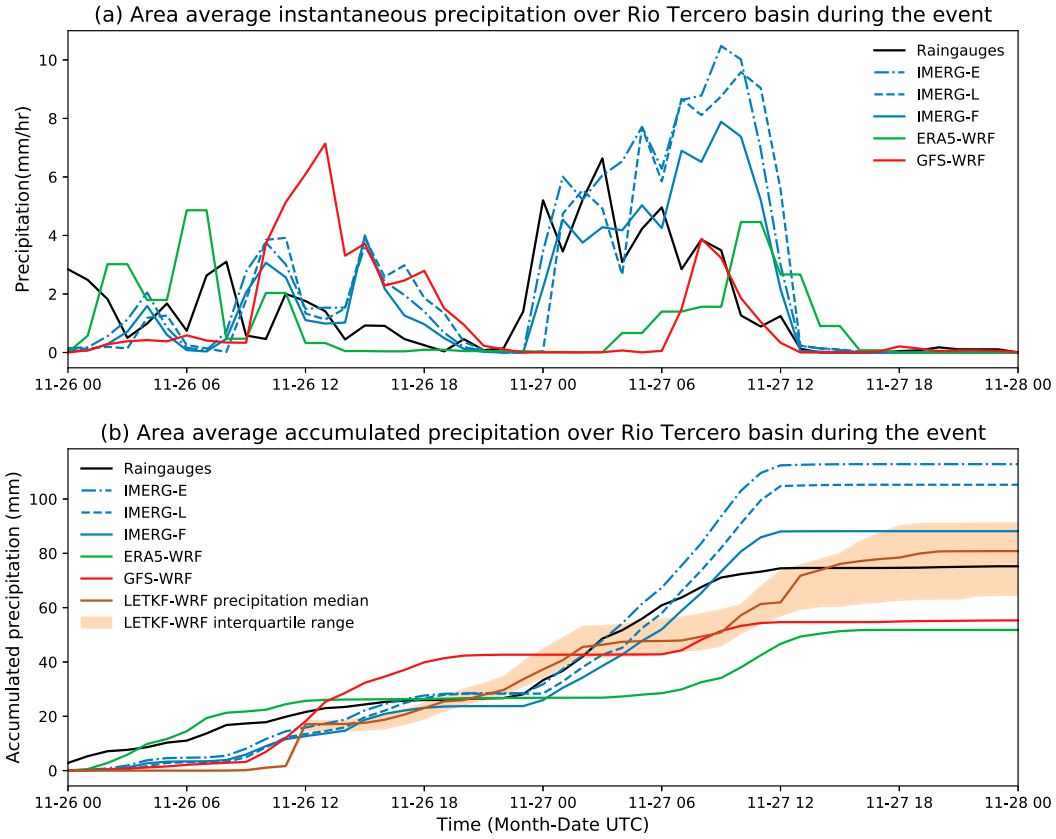

FIG. 12. (a) Area-average precipitation from different precipitation sources available during RELAMPAGO. Area average precipitation from rain gauges is calculated using Thiessen Polygon method. (b) As in (a), but for accumulated precipitation. LETKF–WRF (60-member ensemble) median precipitation and one standard deviation ensemble spread around the median is included in (b).

peak flow amount (RMSE = 105.52 and 101.14 $m^3 s^{-1}$, respectively). ERA5–WRFHydro simulation was comparable to IMERG-F–WRFHydro with similar bias (RMSE = 60.10 $m^3 s^{-1}$). GFS–WRFHydro did not perform well in terms of either timing or magnitude (negative R and NSE). This can again be attributed to over estimation of precipitation by GFS–WRF on 26 November [section 3b(1)]. LETKF–WRFHydro was able to improve the peak flow timing and magnitude (R = 0.61, NSE = 0.42, and RMSE = 82.81), although it was not able to capture the recession.

Overall, negative R and NSE values associated with GFS–WRFHydro indicates low skill of the forecasts on all three rivers. The forecast skill was better in LETKF–WRFHydro (see R and NSE values in Table 5). GFS–WRFHydro has highest RMSE in all three rivers, while LETKF–WRFHydro performs better. LETKF–WRFHydro RMSE is even lower than ERA5–WRFHydro in La Cruz and Quillinzo.

As such, bias in streamflow forecast was significantly lowered when regional atmospheric data assimilated precipitation product was used. The results highlight the importance of using realistic precipitation for flash flood modeling as well as capability of WRF-Hydro as a physics based distributed hydrology model for flood prediction in this region. This modeling framework could be suitable in the region as it was able to achieve NSE values 0.56, 0.60, and 0.62 (in Santa Rosa, La Cruz, and Quillinzo, respectively) with minimal calibration in a hindcast mode (IMERG-F–WRFHydro and 0.42, 0.43, and 0.24 in the same locations in a forecast mode (LETKF–WRFHydro), which are satisfactory given the challenges in subdaily scale forecasting. Critically, we see the potential for using an ensemble system such as LETKF–WRF for hydrologic forecasting purposes. However, it is important to highlight that in addition to the uncertainty coming from the forcing, model parameter related uncertainty in WRF-Hydro (such as the assumption of trapezoidal channel and calculation of channel routing parameters as functions of stream order) can also affect the performance of the hydrologic model.

d. Implications for water management

The simulations and data generated during the field campaigns of RELAMPAGO project have been used intensively for water management in the province of Córdoba, highlighting the collaboration as an important aspect of the project. During this event of 26 November 2018, the information registered in the field was transferred to the province authorities in real time, which allowed an adequate management of the drained volumes (operating valves, gates,

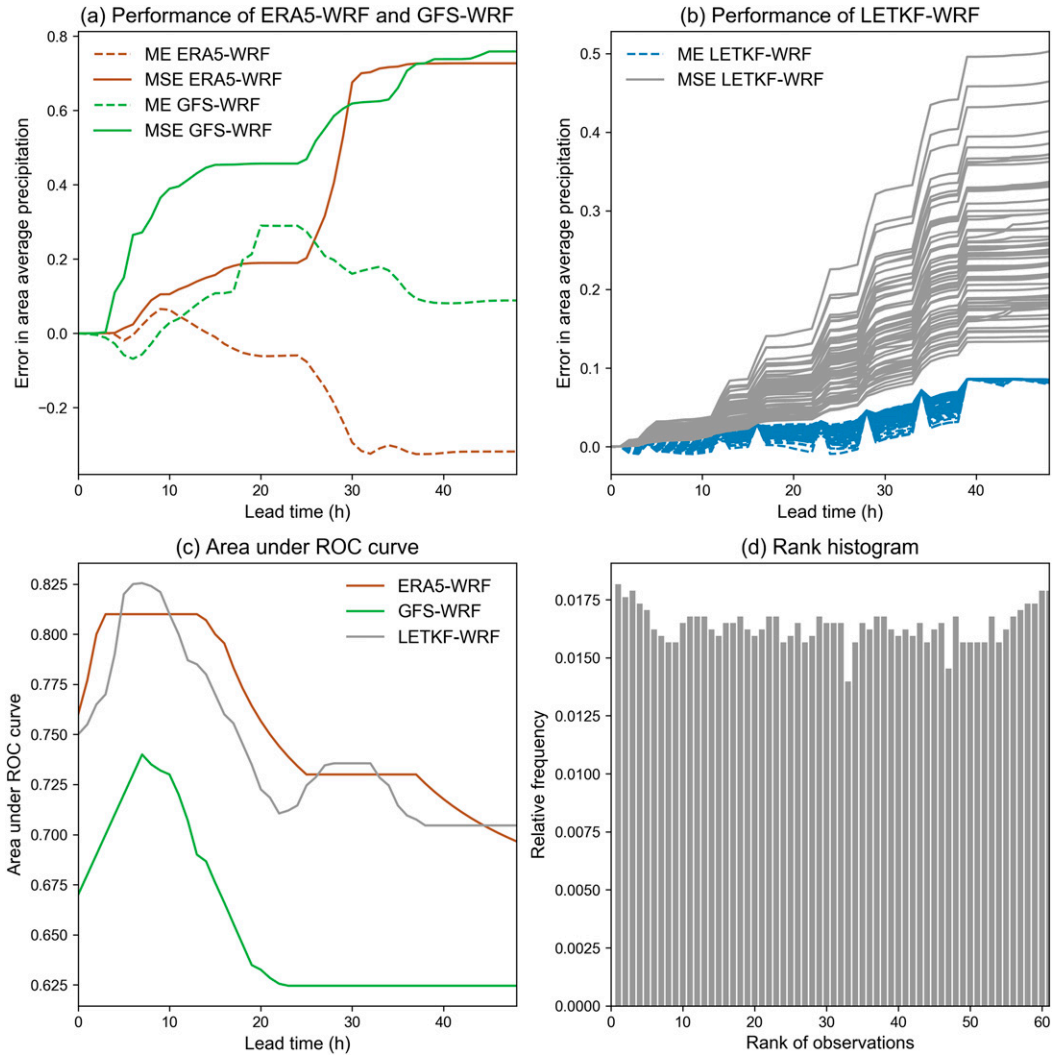

FIG. 13. Verification and skill metrics for the area-average precipitation products with lead time: (a) ME and MSE of ERA5–WRF and GFS–WRF, (b) ME and MSE of LETKF–WRF ensemble members, (c) AROC values for ERA5–WRF, GFS–WRF, and LETKF–WRF median. (d) Rank histogram for LETKF–WRF 60-member ensemble.

etc.) in the different reservoirs of the system, preserving valuable water resources, lives and property in the basin. In addition, the different calibrated models and other tools (together with the meteorological information generated by the models of the RELAMPAGO project) are allowing an effective management of the surface flows drained into the dams. The framework developed in this paper for the Rio Tercero basin is also being implemented in other basins of the province that are vulnerable to the impacts of flash floods due to higher population density and tourism activities.

4. Summary and conclusions

The mountainous region of west central Argentina experiences some of the most severe convection in the world with respect to the frequency of large hail, intense, organized convection, lightning and flash flooding activity. This study is part of the hydrometeorological component of the RELAMPAGO field campaign and focuses on the analysis of an extreme rainfall event during the IOP. The RELAMPAGO Hydrometeorology component had two primary foci: observational and modeling.

Lessons learned from the observational perspective:

- The hydrologic team was able to successfully deploy streamflow observations because we worked in collaboration with weather forecasters. Without the weather forecasters and real-time radar observations, our team would not have been able to reach these remote sites with enough time to monitor the entire hydrologic response. Our collaboration also allowed us to build three stage–discharge

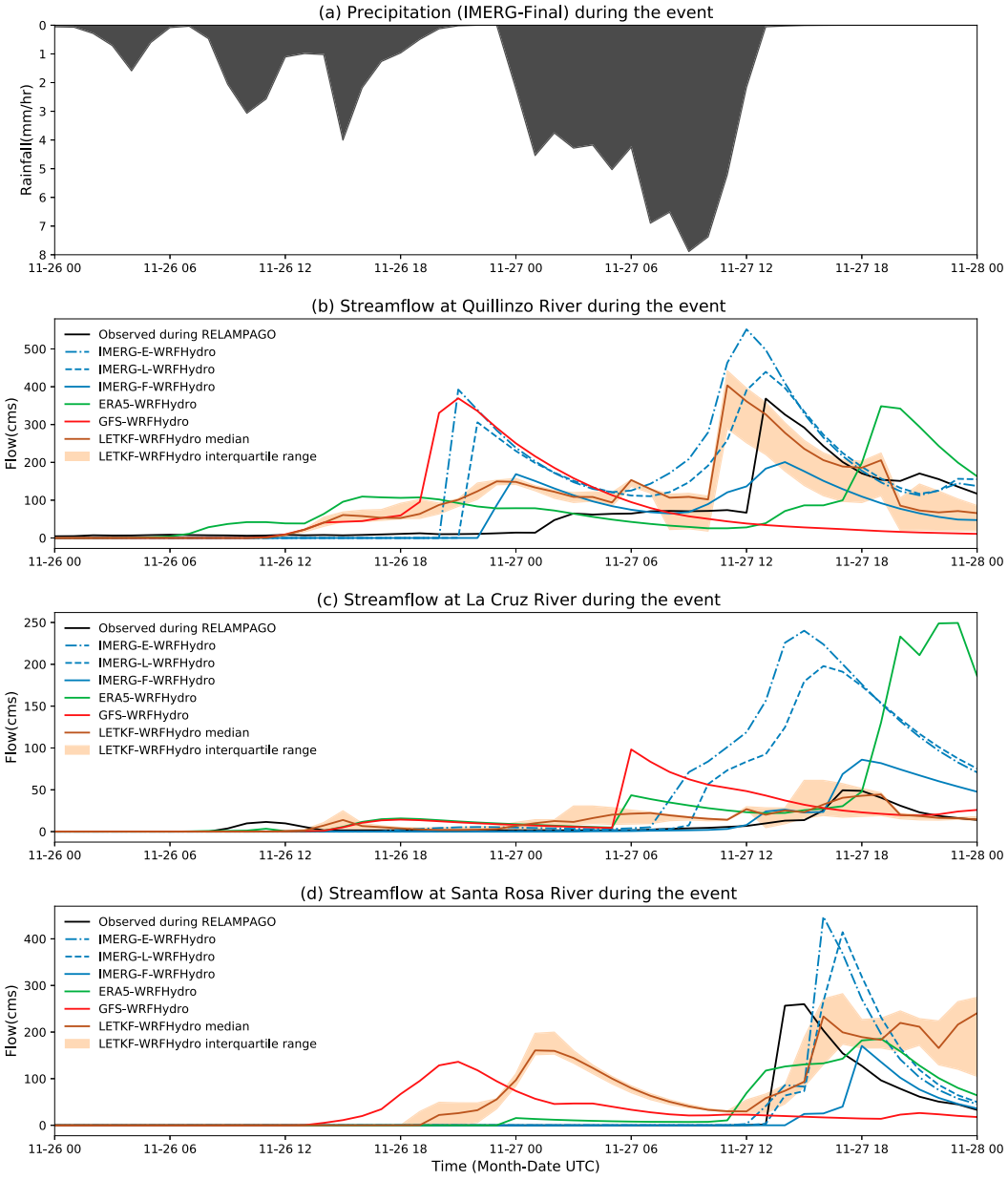

FIG. 14. Streamflow hindcast and forecasting with WRF-Hydro, forced with different forcing data available during RELAMPAGO. Observed streamflow data are estimated with ADCP and LSPIV. (a) Basin-average IMERG-F precipitation during the event. Streamflow estimated by WRF-Hydro while forced with IMERG-E, IMER-L and IMERG-F precipitation, ERA5–WRF precipitation, GFS–WRF precipitation and LETKF–WRF precipitation at (b) Quillinzo, (c) La Cruz, and (d) Santa Rosa.

curves, including extreme flow conditions, within the time of the IOP.

- Traditional streamflow observations (current meters or ADCP) do not work well in these types of rivers because streamflow response is so flashy. For this reason, members of our team have been working with the USGS to improve the use of LSPIV techniques to measure extreme hydrologic response in the high-flow conditions. The recently enhanced LSPIV techniques have allowed us to safely measure the extreme streamflow response and build the rating curve in these previously ungauged basins.
- Our results suggest that near-real-time remotely sensed IMERG precipitation estimates (both IMERG-E and IMERG-L) have substantial bias and should not be used for hydrologic prediction in the region without prior bias correction.
- Observations during IOP found that the time to peak in the rivers Quillinzo, La Cruz, and Santa Rosa were 5–6 h. This information can be used for hazard prevention as this

TABLE 5. Performance metrics (R = correlation coefficient, NSE = Nash–Sutcliffe efficiency, and RMSE = root-mean-square error) of WRF-Hydro based on obtained calibrated parameters for different forcing data.

Statistical metrics	Simulation name	Santa Rosa	La Cruz	Quillinzo
R	IMERF-E–WRFHydro	0.69	0.86	0.58
	IMERG-L–WRFHydro	0.74	0.75	0.73
	IMERG-F–WRFHydro	0.76	0.91	0.74
	ERA5–WRFHydro	0.77	0.51	0.53
	GFS–WRFHydro	−0.13	0.13	−0.22
	LETKF–WRFHydro	0.61	0.77	0.64
RMSE ($m^3 s^{-1}$)	IMERG-E–WRFHydro	105.52	74.92	138.87
	IMERG-L–WRFHydro	101.14	59.55	95.93
	IMERG-F–WRFHydro	58.97	15.95	62.55
	ERA5–WRFHydro	60.10	68.42	96.37
	GFS–WRFHydro	95.26	27.06	146.01
	LETKF–WRFHydro	82.81	8.98	84.81
NSE	IMERG-E–WRFHydro	0.46	0.27	0.15
	IMERG-L–WRFHydro	0.52	0.25	0.40
	IMERG-F–WRFHydro	0.56	0.60	0.62
	ERA5–WRFHydro	0.47	0.14	0.39
	GFS–WRFHydro	−0.03	−0.16	−0.23
	LETKF–WRFHydro	0.42	0.43	0.24

is a touristic region where people flock to the rivers during the summer season when sudden extreme storms can result in rapid rise of the waters and have resulted in loss of life.

Lessons learned from the modeling perspective:

- Adequately representing the hydrologic response of these intense convective storms benefits from a physically based detailed high-resolution model such as WRF-Hydro. In the study area, small differences in representing the storm location can result in large differences related to the streamflow response. In this case, WRF-Hydro has the added benefit of working seamlessly with the weather forecast input data.
- Assimilation of atmospheric data into the WRF using LETKF–WRF improves the precipitation forecast and this results in an improved hydrologic forecast. Furthermore, the ensemble-based approach can provide information about uncertainty in the atmospheric forcing. Based on the encouraging LETKF–WRF initial results, the Argentinian National Meteorological Service is working on the implementation of a high-resolution hourly LETKF–WRF system over southern South America. Regional atmospheric data assimilation with products such as LETKF–WRF could eventually improve probabilistic hydrologic prediction in these short and highly intense rainfall events.
- Further research is needed to assess the added value of a ''coupled'' hydrometeorological modeling system (e.g., coupled WRF-Hydro) and direct assimilation of streamflow measurement to improve the hydrologic modeling (Seo et al. 2003; Rakovec et al. 2015; Li et al. 2015).

Lessons learned from the stakeholders' perspective:

- The results from this work have already been used by the water managers and reservoir operations in the region to make decisions about water release from the reservoirs.
- The Ministry of Public Services from the Córdoba Province Government provided the stage-measurement instruments, and these were installed in collaboration with RELAMPAGO. For this reason, the measurements will be available well beyond the RELAMPAGO field campaign and will be useful for the communities in the region for both water resource management and flood preparedness purposes.

The hydrometeorological observations and modeling during RELAMPAGO were the result of hydrologists working seamlessly with weather forecasters and atmospheric modelers. Equally important was the collaboration between scientists from the United States and Argentina. From the initial design of the experiments, all the way to the final transference of results to stakeholders. This is an important lesson for future international hydrometeorological field campaigns.

Acknowledgments. IMERG, GFS, and ERA5 data are available online. RELAMPAGO data are available from NCAR EOL online data archive. All model outputs, archived on a server maintained by University of Illinois School of Earth, Society, and Environment, are available upon request. Support for this study has been provided by the National Science Foundation (NSF) Grant 1641167 ''RELAMPAGO Hydrometeorology Component: Land Surface Controls on Heavy Precipitation and Flooding in the Carcarañá River Basin, Argentina'' and 1661799 ''Using RELAMPAGO Observations to Understand the Thermodynamic, Kinematic, and Dynamic Processes Leading to Heavy Precipitation.'' We are thankful to the University of Córdoba and the Ministry of Public services form the Córdoba province for providing the streamflow measuring instruments and technology. We acknowledge the Cheyenne HPC resources (doi:10.5065/D6RX99HX) from NCAR's Computational and Information Systems Laboratory, NSF (project code UIUC0012) for the RRR

processing. PIDDEF 16/2014, PICT 2014-1000, PICT 2017-2033, and PICT 2018-3202 partially funded the RRR project. We are also very thankful for all the people involved from NCAR EOL, NCAR RAL, SMN, CIMA, University of Illinois, Colorado State University, University of Buenos Aires, University of Maryland, and RIKEN. We also thank Prof. Praveen Kumar (UIUC) for many fruitful discussions and inputs. We gratefully thank the three reviewers for their valuable comments and suggestions, which helped to improve the paper. The authors declare no conflict of interest.

REFERENCES

Adikari, Y., and J. Yoshitani, 2009: Global trends in water related disasters: An insight for policymakers. International Centre for Water Hazard and Risk Management, UNESCO, 24 pp., https://unesdoc.unesco.org/ark:/48223/pf0000181793.

American Meteorological Society, 2020: Thiessen polygon method. Glossary of Meteorology, https://glossary.ametsoc.org/wiki/Thiessen_polygon_method.

Ashley, S. T., and W. S. Ashley, 2008: Flood fatalities in the United States. *J. Appl. Meteor. Climatol.*, **47**, 805–818, https://doi.org/10.1175/2007JAMC1611.1.

Band, L. E., T. Hwang, T. C. Hales, J. Vose, and C. Ford, 2012: Ecosystem processes at the watershed scale: Mapping and modeling ecohydrological controls of landslides. *Geomorphology*, **137**, 159–167, https://doi.org/10.1016/j.geomorph.2011.06.025.

Broxton, P., P. A. Troch, M. Schaffner, C. Unkrich, and D. Goodrich, 2014: An all-season flash flood forecasting system for real-time operations. *Bull. Amer. Meteor. Soc.*, **95**, 399–407, https://doi.org/10.1175/BAMS-D-12-00212.1.

Buehner, M., J. Morneau, and C. Charette, 2013: Four-dimensional ensemble-variational data assimilation for global deterministic weather prediction. *Nonlinear Processes Geophys.*, **20**, 669–682, https://doi.org/10.5194/npg-20-669-2013.

CISL, 2019: Cheyenne: HPE/SGI ICE XA System (University Community Computing). NCAR, https://doi.org/10.5065/D6RX99HX.

Clark, M. P., and Coauthors, 2008: Framework for Understanding Structural Errors (FUSE): A modular framework to diagnose differences between hydrological models. *Water Resour. Res.*, **44**, W00B02, https://doi.org/10.1029/2007WR006735.

Colautti, F., 2007: Río Tercero: cuál es el riesgo de inundación. Lavoz.com.ar, 25 January, http://archivo.lavoz.com.ar/07/01/25/secciones/zonacentro/nota.asp?nota_id=38409.

Dee, D. P., and Coauthors, 2011: The ERA-Interim reanalysis: Configuration and performance of the data assimilation system. *Quart. J. Roy. Meteor. Soc.*, **137**, 553–597, https://doi.org/10.1002/qj.828.

Dillon, M. E., and Coauthors, 2016: Application of the WRFLETKF data assimilation system over southern South America: Sensitivity to model physics. *Wea. Forecasting*, **31**, 217–236, https://doi.org/10.1175/WAF-D-14-00157.1.

Fenicia, F., D. Kavetski, and H. H. G. Savenije, 2011: Elements of a flexible approach for conceptual hydrological modeling. 1: Motivation and theoretical development. *Water Resour. Res.*, **47**, W11510, https://doi.org/10.1029/2010WR010174.

Fersch, B., A. Senatore, B. Adler, J. Arnault, M. Mauder, K. Schneider, I. Völksch, and H. Kunstmann, 2020: 2019: High-resolution fully coupled atmospheric–hydrological modeling: A cross-compartment regional water and energy cycle evaluation. *Hydrol. Earth Syst. Sci.*, **24**, 2457–2481, https://doi.org/10.5194/hess-24-2457-2020.

French, J. G., R. Ing, S. Von Allmen, and R. Wood, 1983: Mortality from flash floods: A review of the National Weather Service reports, 1969–81. *Public Health Rep.*, **98** (6), 584–588.

Furnari, L., G. Mendicino, and A. Senatore, 2020: Hydrometeorological ensemble forecast of a highly localized convective event in the Mediterranean. *Water*, **12**, 1545, https://doi.org/10.3390/w12061545.

Georgakakos, K. P., and M. D. Hudlow, 1984: Quantitative precipitation forecast techniques for use in hydrologic forecasting. *Bull. Amer. Meteor. Soc.*, **65**, 1186–1200, https://doi.org/10.1175/1520-0477(1984)065<1186:QPFTFU>2.0.CO;2.

Gochis, D. J., and F. Chen, 2003: Hydrological enhancements to the community Noah land surface model. NCAR Scientific Tech. Rep. TN-454+STR, 77 pp., https://doi.org/10.5065/D60P0X00.

——, W. Yu, K. Sampson, A. Dugger, J. McCreight, Y. Zhang, and K. Ikeda, 2015: Multi-scale model analysis and hindcast of the 2013 Colorado Flood. *EGU General Assembly*, Vienna, Austria, European Geophys. Union, 7531.

——, and Coauthors, 2018: The WRF-Hydro modeling system technical description (version 5.0). NCAR Tech. Note, 107 pp., https://ral.ucar.edu/sites/default/files/public/WRF-HydroV5TechnicalDescription.pdf.

Gruntfest, E., and C. J. Huber, 1991: Toward a comprehensive national assessment of flash flooding in the United States. *Episodes*, **14**, 26–34.

Herrero, H. S., J. M. D. Lozada, C. M. García, R. N. Szupiany, J. Best, and M. Pagot, 2018: The influence of tributary flow density differences on the hydrodynamic behavior of a confluent meander bend and implications for flow mixing. *Geomorphology*, **304**, 99–112, https://doi.org/10.1016/j.geomorph.2017.12.025.

Hersbach, H., and D. Dee, 2016: ERA5 reanalysis is in production. *ECMWF Newsletter*, No. 147, ECMWF, Reading, United Kingdom, 7, https://www.ecmwf.int/sites/default/files/elibrary/2016/16299-newsletter-no147-spring-2016.pdf.

Hunt, B. R., E. J. Kostelich, and I. Szunyogh, 2007: Efficient data assimilation for spatiotemporal chaos: A local ensemble transform Kalman filter. *Physica D*, **230**, 112–126, https://doi.org/10.1016/j.physd.2006.11.008.

Lange, J., and C. Leibundgut, 2000: Non-calibrated arid zone rainfall-runoff modelling. *IAHS Publ.*, **261**, 45–5, http://hydrologie.org/redbooks/a261/iahs_261_0045.pdf 2.

Le Coz, J., M. Jodeau, A. Hauet, B. Marchand, and R. Boursicaud, 2014: Image-based velocity and discharge measurements in field and laboratory river engineering studies using the free FUDAA-LSPIV software. *River Flow 2014*, A. J. Schleiss et al., Eds., CRC Press, 7 pp.

Li, Y., D. Ryu, A. W. Western, and Q. Wang, 2015: Assimilation of stream discharge for flood forecasting: Updating a semi-distributed model with an integrated data assimilation scheme. *Water Resour. Res.*, **51**, 3238–3258, https://doi.org/10.1002/2014WR016667.

Lin, P., L. J. Hopper, Z.-L. Yang, M. Lenz, and J. W. Zeitler, 2018a: Insights into hydrometeorological factors constraining flood prediction skill during the May and October 2015 Texas Hill Country flood events. *J. Hydrometeor.*, **19**, 1339–1361, https://doi.org/10.1175/JHM-D-18-0038.1.

——, M. A. Rajib, Z.-L. Yang, M. Somos-Valenzuela, V. Merwade, D. R. Maidment, Y. Wang, and L. Chen, 2018b: Spatiotemporal evaluation of simulated evapotranspiration and streamflow over Texas using the WRF-Hydro-RAPID modeling framework. *J. Amer. Water Resour. Assoc.*, **54**, 40–54, https://doi.org/10.1111/1752-1688.12585.

Michaud, J., and S. Sorooshian, 1994: Comparison of simple versus complex distributed runoff models on a midsized semiarid watershed. *Water Resour. Res.*, **30**, 593–605, https://doi.org/10.1029/93WR03218.

Miyoshi, T., and M. Kunii, 2011: The local ensemble transform Kalman filter with the Weather Research and Forecasting Model: Experiments with real observations. *Pure Appl. Geophys.*, **169**, 321–333, https://doi.org/10.1007/s00024-011-0373-4.

Moore, R., and R. Clarke, 1981: A distribution function approach to rainfall runoff modeling. *Water Resour. Res.*, **17**, 1367–1382, https://doi.org/10.1029/WR017i005p01367.

Moriasi, D. N., J. G. Arnold, M. W. Van Liew, R. L. Bingner, R. D. Harmel, and T. L. Veith, 2007: Model evaluation guidelines for systematic quantification of accuracy in watershed simulations. *Trans. ASABE*, **50**, 885–900, https://doi.org/10.13031/2013.23153.

Mueller, D. S., C. R. Wagner, M. S. Rehmel, K. A. Oberg, and F. Rainville, 2013: Measuring discharge with acoustic Doppler current profilers from a moving boat. USGS Techniques and Methods Rep. 3-A22, 95 pp., https://doi.org/10.3133/tm3A22.

Mulholland, J. P., S. W. Nesbitt, R. J. Trapp, K. L. Rasmussen, and P. V. Salio, 2018: Convective storm life cycle and environments near the Sierras de Cordoba, Argentina. *Mon. Wea. Rev.*, **146**, 2541–2557, https://doi.org/10.1175/MWR-D-18-0081.1.

——, ——, and ——, 2019: A case study of terrain influences on upscale convective growth of a supercell. *Mon. Wea. Rev.*, **147**, 4305–4324, https://doi.org/10.1175/MWR-D-19-0099.1.

Muste, M., I. Fujita, and A. Hauet, 2008: Large-scale particle image velocimetry for measurements in riverine environments. *Water Resour. Res.*, **44**, W00D19, https://doi.org/10.1029/2008WR006950.

Naabil, E., B. Lamptey, J. Arnault, A. Olufayo, and H. Kunstmann, 2017: Water resources management using the WRF-Hydro modelling system: Case-study of the Tono Dam in West Africa. *J. Hydrol. Reg. Stud.*, **12**, 196–209, https://doi.org/10.1016/j.ejrh.2017.05.010.

Nash, J. E., and J. V. Sutcliffe, 1970: River flow forecasting through conceptual models, Part I – A discussion of principles. *J. Hydrol.*, **10**, 282–290, https://doi.org/10.1016/0022-1694(70)90255-6.

Nesbitt, S., 2016: RELAMPAGO white paper. 6 pp., https://drive.google.com/file/d/0B6Z5EcBIjxY2dWo4TFFIRWZMMTg/view.

Niu, G. Y., and Coauthors, 2011: The community Noah land surface model with multiparameterization options (Noah-MP): 1. Model description and evaluation with local-scale measurements. *J. Geophys. Res.*, **116**, D12109, https://doi.org/10.1029/2010JD015139.

Noji, E. K., and C. Y. Lee, 2005: Disaster preparedness. *Environmental Health: From Global to Local*, 1st ed. H. Frumkin, Ed., Jossey-Bass Publisher, 745–780.

Norbiato, D., M. Borga, S. Degli Esposti, E. Gaume, and S. Anquetin, 2008: Flash flood warning based on rainfall thresholds and soil moisture conditions: An assessment for gauged and ungauged basins. *J. Hydrol.*, **362**, 274–290, https://doi.org/10.1016/j.jhydrol.2008.08.023.

Pal, S., H.-I. Chang, C. L. Castro, and F. Dominguez, 2019: Credibility of convection-permitting modeling to improve seasonal precipitation forecasting in the southwestern United States. *Front Earth Sci.*, **7**, 11, https://doi.org/10.3389/feart.2019.00011.

Patalano, A., C. García, and A. Rodriguez, 2017: Rectification of Image Velocity Results (RIVeR): A simple and user-friendly toolbox for large scale water surface particle image velocimetry (PIV) and particle tracking velocimetry (PTV). *Comput. Geosci.*, **109**, 323–330, https://doi.org/10.1016/j.cageo.2017.07.009.

Prein, A. F., and Coauthors, 2015: A review on regional convection-permitting climate modeling: Demonstrations, prospects and challenges. *Rev. Geophys.*, **53**, 323–361, https://doi.org/10.1002/2014RG000475.

Rakovec, O., A. H. Weerts, J. Sumihar, and R. Uijlenhoet, 2015: Operational aspects of asynchronous filtering for flood forecasting. *Hydrol. Earth Syst. Sci.*, **19**, 2911–2924, https://doi.org/10.5194/hess-19-2911-2015.

Rasmussen, K. L., and R. A. Houze Jr., 2011: Orogenic convection in subtropical South America as seen by the TRMM satellite. *Mon. Wea. Rev.*, **139**, 2399–2420, https://doi.org/10.1175/MWR-D-10-05006.1.

——, and ——, 2016: Convective initiation near the Andes in subtropical South America. *Mon. Wea. Rev.*, **144**, 2351–2374, https://doi.org/10.1175/MWR-D-15-0058.1.

——, M. D. Zuluaga, and R. A. Houze Jr., 2014: Severe convection and lightning in subtropical South America. *Geophys. Res. Lett.*, **41**, 7359–7366, https://doi.org/10.1002/2014GL061767.

——, M. M. Chaplin, M. D. Zuluaga, and R. A. Houze Jr., 2016: Contribution of extreme convective storms to rainfall in South America. *J. Hydrometeor.*, **17**, 353–367, https://doi.org/10.1175/JHM-D-15-0067.1.

Reed, S., J. Schaake, and Z. Zhang, 2007: A distributed hydrologic model and threshold frequency-based method for flash flood forecasting at ungauged locations. *J. Hydrol.*, **337**, 402–420, https://doi.org/10.1016/j.jhydrol.2007.02.015.

Rozalis, S., E. Morin, Y. Yair, and C. Price, 2010: Flash flood prediction using an uncalibrated hydrological model and radar rainfall data in a Mediterranean watershed under changing hydrological conditions. *J. Hydrol.*, **394**, 245–255, https://doi.org/10.1016/j.jhydrol.2010.03.021.

Ryu, Y., Y. J. Lim, H. S. Ji, H. H. Park, E. C. Chang, and B. J. Kim, 2017: Applying a coupled hydrometeorological simulation system to flash flood forecasting over the Korean Peninsula. *Asia-Pac. J. Atmos. Sci.*, **53**, 421–430, https://doi.org/10.1007/s13143-017-0045-0.

Salio, P., M. Nicolini, and C. Saulo, 2002: Chaco low-level jet events characterization during the austral summer season. *J. Geophys. Res.*, **107**, 4816, https://doi.org/10.1029/2001JD001315.

——, ——, and E. J. Zipser, 2007: Mesoscale convective systems over southeastern South America and their relationship with the South American low-level jet. *Mon. Wea. Rev.*, **135**, 1290–1309, https://doi.org/10.1175/MWR3305.1.

Sauer, V. B., and D. P. Turnipseed, 2010: Stage measurement at gaging stations. USGS Techniques and Methods Rep. 3-A7, 45 pp., https://doi.org/10.3133/tm3A7.

Saulo, A. C., M. E. Seluchi, and M. Nicolini, 2004: A case study of a Chaco low-level jet event. *Mon. Wea. Rev.*, **132**, 2669–2683, https://doi.org/10.1175/MWR2815.1.

——, J. Ruiz, and Y. G. Skabar, 2007: Synergism between the low-level jet and organized convection at its exit region. *Mon. Wea. Rev.*, **135**, 1310–1326, https://doi.org/10.1175/MWR3317.1.

Schneider, U., A. Becker, A. Meyer-Christoffer, M. Ziese, and B. Rudolf, 2011: Global Precipitation Analysis Products of the GPCC. Global Precipitation Climatology Centre, DWD, 13 pp., https://www.dwd.de/EN/ourservices/gpcc/reports_publications/GPCC_intro_products_2011.pdf?__blob=publicationFile&v=3.

Senatore, A., G. Mendicino, D. J. Gochis, W. Yu, D. Yates, and H. Kunstmann, 2015: Fully coupled atmosphere-hydrology

simulations for the central Mediterranean: Impact of enhanced hydrological parameterization for short and long time scales. *J. Adv. Model. Earth Syst.*, **7**, 1693–1715, https://doi.org/10.1002/2015MS000510.

——, L. Furnari, and G. Mendicino, 2020: Impact of high-resolution sea surface temperature presentation on the forecast of small Mediterranean catchments' hydrological responses to heavy precipitation. *Hydrol. Earth Syst. Sci.*, **24**, 269–291, https://doi.org/10.5194/hess-24-269-2020.

Seo, D. J., V. Koren, and N. Cajina, 2003: Real-time variational assimilation of hydrologic and hydrometeorological data into operational hydrologic forecasting. *J. Hydrometeor.*, **4**, 627–641, https://doi.org/10.1175/1525-7541(2003)004<0627:RVAOHA>2.0.CO;2.

Sivapalan, M., and Coauthors, 2003: IAHS decade on Predictions in Ungauged Basins (PUB), 2003–2012: Shaping an exciting future for the hydrological sciences. *Hydrol. Sci. J.*, **48**, 857–880, https://doi.org/10.1623/hysj.48.6.857.51421.

Skamarock, W. C., and Coauthors, 2008: A description of the Advanced Research WRF version 3. NCAR Tech. Note NCAR/TN-475+STR, 113 pp., https://doi.org/10.5065/D68S4MVH.

Smith, M. B., and Coauthors, 2012: Results of the DMIP 2 Oklahoma experiments. *J. Hydrol.*, **418–419**, 17–48, https://doi.org/10.1016/j.jhydrol.2011.08.056.

Tao, J., and A. P. Barros, 2013: Prospects for flash flood forecasting in mountainous regions—An investigation of Tropical Storm Fay in the southern Appalachians. *J. Hydrol.*, **506**, 69–89, https://doi.org/10.1016/j.jhydrol.2013.02.052.

——, D. Wu, J. Gourley, S. Q. Zhang, W. Crow, C. Peters-Lidard, and A. P. Barros, 2016: Operational hydrological forecasting during the IPHEx-IOP campaign–Meet the challenge. *J. Hydrol.*, **541**, 434–456, https://doi.org/10.1016/j.jhydrol.2016.02.019.

Tarek, M., F. P. Brissette, and R. Arsenault, 2020: Evaluation of the ERA5 reanalysis as a potential reference dataset for hydrological modeling over North-America. *Hydrol. Earth Syst. Sci.*, **24**, 2527–2544, https://doi.org/10.5194/hess-24-2527-2020.

TRMM, 2011: TRMM (TMPA) Rainfall Estimate L3 3 hour 0.25 degree × 0.25 degree V7 (TRMM_3B42). GES DISC, accessed 16 May 2020, https://doi.org/10.5067/TRMM/TMPA/3H/7.

Varlas, G., and Coauthors, 2019: A multi-platform hydrometeorological analysis of the flash flood event of 15 November 2017 in Attica, Greece. *Remote Sens.*, **11**, 45, https://doi.org/10.3390/rs11010045.

Vidal, L., 2014: Convección extrema sobre Sudamérica: estructura interna, ciclos de vida e influencia de la topografía en la iniciación. PhD. dissertation, Universidad de Buenos Aires, 275 pp.

Viterbo, F., and Coauthors, 2020: A multiscale, hydrometeorological forecast evaluation of national water model forecasts of the May 2018 Ellicott City, Maryland, flood. *J. Hydrometeor.*, **21**, 475–499, https://doi.org/10.1175/JHM-D-19-0125.1.

Wilks, D. S., 2011: Forecast verification. *Statistical Methods in the Atmospheric Sciences*, 3rd ed. International Geophysics Series, Vol. 100, Academic Press, 301–394.

Yucel, I., A. Onen, K. K. Yilmaz, and D. J. Gochis, 2015: Calibration and evaluation of a flood forecasting system: Utility of numerical weather prediction model, data assimilation and satellite-based rainfall. *J. Hydrol.*, **523**, 49–66, https://doi.org/10.1016/j.jhydrol.2015.01.042.

Zipser, E. J., D. J. Cecil, C. Liu, S. W. Nesbitt, and D. P. Yorty, 2006: Where are the most intense thunderstorms on Earth? *Bull. Amer. Meteor. Soc.*, **87**, 1057–1072, https://doi.org/10.1175/BAMS-87-8-1057.